

Research

DECOVALEX-THMC Project

Task C

Excavation Damaged Zone (EDZ) in argillaceous rock at Tournemire site (France)

Report of Task C1

Compiled by:

A. Rejeb, Institute of Radioprotection and Nuclear Safety, France

O. Stephansson, GeoForschungsZentrum-Potsdam, Germany

February 2007

Research

DECOVALEX-THMC Project

Task C

Excavation Damaged Zone (EDZ) in argillaceous rock at Tournemire site (France)

Report of Task C1

Compiled by:

A. Rejeb, Institute of Radioprotection and Nuclear Safety, France
O. Stephansson, GeoForschungsZentrum-Potsdam, Germany

With contributions from:

A. Millard, A. Rejeb, CEA/IRSN team
G. Ziefle, M. Kohlmeier, J. Maßmann and W. Zielke, ISEB/BGR team,
S. Uehara, A. Kobayashi, M. Chijimatsu, and T. Fujita, KU/JAEA team

February 2007



This report concerns a study which has been conducted for the Project DECOVALEX-THMC. The conclusions and viewpoints presented in the report are those of the author/authors and do not necessarily coincide with those of the SKI.

Foreword

The DECOVALEX-THMC project is an ongoing international co-operative project that was started in 2004 to support the development of mathematical models of coupled Thermal (T), Hydrological (H), Mechanical (M) and Chemical (C) processes in geological media for siting potential nuclear fuel waste repositories. The general objective is to characterise and evaluate the coupled THMC processes in the near field and far field of a geological repository and to assess their impact on performance assessment:

- during the three phases of repository development: excavation phase, operation phase and post-closure phase;
- for three different rock types: crystalline, argillaceous and tuff;
- with specific focus on the issues of: Excavation Damaged Zone (EDZ), permanent property changes of rock masses, and glaciation and permafrost phenomena.

The project involves a large number of research teams supported by radioactive waste management agencies or governmental regulatory bodies in Canada, China, Finland, France, Germany, Japan, Sweden and USA, who conducted advanced studies and numerical modelling of coupled THMC processes under five tasks:

- **Task A:** Influence of near field coupled THM phenomena on performance assessment, initiated by CNSC, Canada.
- **Task B:** The Excavation Disturbed Zone (EDZ). MHC studies of the EDZ, initiated by SKB, Sweden.
- **Task C:** Excavation Damaged Zone (EDZ) in the argillaceous Tournemire site, France, initiated by IRSN, France.
- **Task D:** Permanent permeability/porosity changes due to THM and THM processes, initiated Department of Energy, USA.
- **Task E:** THM Processes Associated with Long-term Climate Change: Glaciations case study, initiated by OPG, Canada.

Work defined in these five tasks are divided into different phases or steps so that the progress can be monitored and achievements documented in project reports.

The present report presents the definition, achievements and outstanding issues of the phase 1 of Task C, Task C1, concerning a description and definition of Task C, EDZ characterization from geological mapping and permeability measurements and numerical modelling results.

Lanru Jing, Fritz Kautsky, Ove Stephansson and Chin-Fu Tsang

Stockholm, Sweden
February 2007

Summary

This report describes the results of Task C1 of the international DECOVALEX–THMC project devoted to Excavation Damage Zone (EDZ) in argillaceous rock at the Tournemire site in France. Task C of the project is aimed to understand the physical phenomena induced by excavation in the argillaceous rock. The task is to develop adequate numerical models for interpretation of observed damaged zones around three different openings excavated at different time at the Tournemire site. The research teams are asked to model the evolution of the EDZ with time and to compare the results with measurements performed at the site.

Three research teams are participating in this task:

- CEA (Commissariat of Atomic Energy, France) and the IRSN (Institute of Radioprotection and Nuclear safety, France) ;
- ISEB (Institute of Fluid Mechanics and Computer Applications in Civil Engineering, University of Hanover, Germany) supported by the BGR (Federal Institute for Geosciences and Natural Resources, Germany);
- KU (Department of Urban and Environmental Engineering, Kyoto University, Japan) supported by the JAEA (Japan Atomic Energy Agency, Japan).

This report presents a description and definition of Task C including a geological description of the site, the geomechanical characterisation of the argillaceous rocks and in particular the stress field, mechanical properties and hydraulic properties. Thereafter, the EDZ characterization from geological mapping and permeability measurements are presented. The EDZ in the 100 years old tunnel drilled manually and with its reinforcement of limestone blocks is very different from the EDZ observed in drifts excavated with road-headers 3 and 10 years ago.

According to the task definition, Task C1 concerns the understanding of the EDZ development around the 100 years old tunnel. The failure mechanism should be identified by analysing the in situ stress field and the orientation of the bedding planes with respect to the axis of the tunnel and the degree of anisotropy. Numerical models have to be developed to predict the extent of the EDZ around the tunnel. The results of the calculations using various approaches should be compared with measured data in order to understand the physical processes and validate the computer models used in the simulations.

The CEA/IRSN team contribution to Task C1 concerns three calculations: a pure mechanical calculation, a coupled hydro-mechanical calculation with saturated rock, and coupled hydro-mechanical calculation with unsaturated rock. The EDZ around the tunnel has been estimated on the basis of a post-processing of the stress calculations, using Mohr-Coulomb failure criterion. These calculations were performed by using the CEA finite element code CASTEM, which can simulate fully coupled THM processes. All the results from the calculations show that an EDZ around the tunnel can only be predicted if we consider mechanical rock properties lower than those measured in laboratory. However, none of the predictions provided the shape and the real extent of the observed EDZ in the tunnel. The evaluation of the EDZ by a simple post-processing technique does not account for the irreversible effect of damage on the mechanical as well as hydraulic behaviour of the argillite.

The ISEB/BGR team performed the simulations by using the finite element code Rock Flow. The team simulated three cases where the influence of capillary pressure,

swelling and initial stresses were considered. Result of the simulation of Case 1 (influence of capillary pressure) shows, that a change of saturation at the boundary of the tunnel influences an area around the tunnel with time. In the near field of the tunnel, the effect of seasonal fluctuation is high. This result is influenced by the boundary conditions, the permeability and the relation between the capillary pressure and the saturation. Case 2 (influence of swelling) incorporates the swelling or shrinking of the argillite. These effects have significant influence on the stresses and displacements in the area around the tunnel. Saturation causes swelling of the material and an increase of stresses. Case 3 (consideration of initial stress field) includes the significant magnitude of the initial stress field in the simulation. Close to the tunnel, zones with high tensile stresses can be observed. The appearance of fractures in the near field of the tunnel, caused by tensile stresses, is plausible.

The KU/JAEA team uses the 3-D finite element code THAMES. Mechanical modelling with isotropic and anisotropic elastic properties and Mohr-Coulomb failure criterion were performed. The results of mechanical modelling indicated that no failure zone is obtained for modelling cases using isotropic and anisotropic elastic properties and Mohr-Coulomb failure criteria derived from peak stresses. Therefore, other mechanisms to explain the fracture zone observed at the tunnel wall must be developed and applied. The results of hydraulic modelling suggest that the change of saturation ratio at the tunnel wall could affect saturation ratio of a domain to a depth of a few meters from the tunnel wall after one year. This prediction supports the hypothesis that seasonal changes of humidity in the tunnel causes swelling-shrinking of the rock in a domain within several tens of cm from tunnel wall.

Following a discussion and an attempt to compare the results of the research teams, it is concluded that conventional elastic isotropic and anisotropic approaches are unable to predict the failure around the tunnel and that other time-dependent visco-elastic and time dependent damage models must be applied to simulate EDZ in argillite. New information about the extent and characteristics of the EDZ in the drifts excavated 3 respectively 10 years ago at the site are now presented to the research teams in the preparation of modelling the evaluation of EDZ with time according to the definition of Task C2.

Content

Foreword

Summary

	Page
1. Introduction	1
2. Site description and definition of Task C	3
2.1 The Tournemire site.....	3
2.2 Geomechanical characterisation.....	5
2.3 EDZ characterisation	7
2.4 Definition of task C.....	10
2.5 Detail description of Task C1	11
3. EDZ modelling by CEA/IRSN team	13
3.1 Introduction.....	13
3.2 Data and assumptions	13
3.3 Mechanical calculations.....	16
3.4 Hydro-mechanical calculations with saturated conditions	18
3.5 Hydro-mechanical calculations with unsaturated conditions	20
3.6 Synthesis	22
4. EDZ modelling by ISEB/BGR team	25
4.1 Introduction.....	25
4.2 Governing equations	25
4.3 Material properties	28
4.4 Definition of simulated cases.....	29
4.5 Results of simulated cases	30
4.6 Synthesis	33
5. EDZ modelling by KU/JAEA team.....	35
5.1 Introduction.....	35
5.2 Code developments.....	35
5.3 Mechanical modelling.....	36
5.4 Hydraulic modelling at unsaturated conditions	38
5.5 Synthesis	39
6. Discussion and conclusion	40
7. Perspective.....	42
References	42

1 Introduction

The DECOVALEX-THMC is the fourth stage of an ongoing international co-operative project to support the development of mathematical models of coupled Thermal (T), Hydrological (H), Mechanical (M) and Chemical (C) processes in geological media for potential nuclear fuel waste repositories.

The general objective is to characterise and evaluate the coupled THMC processes in the near field and far field of a geological repository and their impact on performance assessment:

- during the three phases of a repository: excavation, operation and post-closure;
- for the three rocks types: crystalline, argillaceous and tuff;
- for the issues of: Excavation Damaged Zone (EDZ), permanent property changes of rock masses, and glaciation, deglaciation and permafrost phenomena.

The project was initiated in January 2004 and will last until end of 2007. The participating organisations assemble their research teams to study the five tasks listed below:

- **Task A:** Influence of near field coupled THM phenomena on performance assessment, initiated by T. S. Nguyen, CNSC, Canada.
- **Task B:** The Excavation Disturbed Zone (EDZ). MHC studies of the EDZ, initiated by J. A. Hudson REC, UK and R. Christiansson, SKB, Sweden.
- **Task C:** Excavation Damaged Zone (EDZ) in the argillaceous Tournemire site, France, initiated by A. Rejeb, IRSN, France.
- **Task D:** Permanent permeability/porosity changes due to THC and THM processes, initiated by D. Barr, Office of Repository Development, U.S. Department of Energy, USA.
- **Task E:** THM Processes Associated with Long-term Climate Change: Glaciations case study, initiated by M. Jenson, Ontario Power Generation, Canada.

The present report is on Task C, which is based on an on-going research programme of the Institute of Radioprotection and Nuclear Safety (IRSN), France at the Tournemire site for studying the fluid transport processes, the site properties and the EDZ effects in argillaceous rock. The task is aimed to understand the physical phenomena induced by excavation in the argillaceous medium, and to develop adequate numerical models for interpretation of observed damaged zones around openings. At this site, three openings were constructed at three times in the past (100, 10, 3 years), and research teams are asked to model the evolution of the EDZ with time and to compare the results with measurements. The work is focused on three issues: (a) the extent of the EDZ around openings; (b) the EDZ properties and (c) advancement of modelling capabilities for EDZ extent and properties.

Three research teams are participating in this task:

- CEA (Commissariat of Atomic Energy, France) and IRSN (Institute of Radioprotection and Nuclear safety, France) ;
- ISEB (Institute of Fluid Mechanics and Computer Applications in Civil Engineering, University of Hanover, Germany) supported by BGR (Federal Institute for Geosciences and Natural Resources, Germany);
- KU (Department of Urban and Environmental Engineering, Kyoto University, Japan) supported by JAEA (Japan Atomic Energy Agency, Japan).

This report presents the task definition with site description, the modelling approaches developed by each research team and the main results and conclusions of the first step of Task C, which is an understanding and modelling of EDZ around the oldest tunnel (100 years).

2 Site description and definition of Task C

2.1 The Tournemire site

The Institute for Radioprotection and Nuclear Safety has a mission of research and development of expertise in safety assessment for deep underground storage of nuclear waste for French governmental authorities. It has selected the Tournemire site in order to study the confining properties of argillaceous media. A multidisciplinary research programme has been conducted for several years, including geological, hydrogeological, geochemical and geomechanical investigations (Boisson et al., 1988).

The research programme is dedicated to the evaluation of fluid migration through the argillaceous formation, as well as the characterisation and long-term behaviour of the excavation damage zone (EDZ) in the underground openings.

The Tournemire site was selected because an old 2 km long railway tunnel gives access to the argillaceous formation located between two limestone layers. The tunnel was excavated manually in 1881 by using a pneumatic engine.

The first study at this site was initiated in 1990 with six vertical boreholes drilled in the tunnel (figure 2.1) to analyse the geological setting. In order to analyse the hydraulic and geochemical perturbations due to the tunnel excavation, eight radial boreholes were drilled in 1994 around the tunnel axis. In 1996, two 30 m long horizontal drifts were excavated perpendicular to the tunnel (Figure 2.1). The excavation was made with a road header under dry conditions. More recently, in 2003, another 40 m long, horizontal drift was excavated perpendicular to the tunnel to carry out a mine-by-test and EDZ characterisation tests.

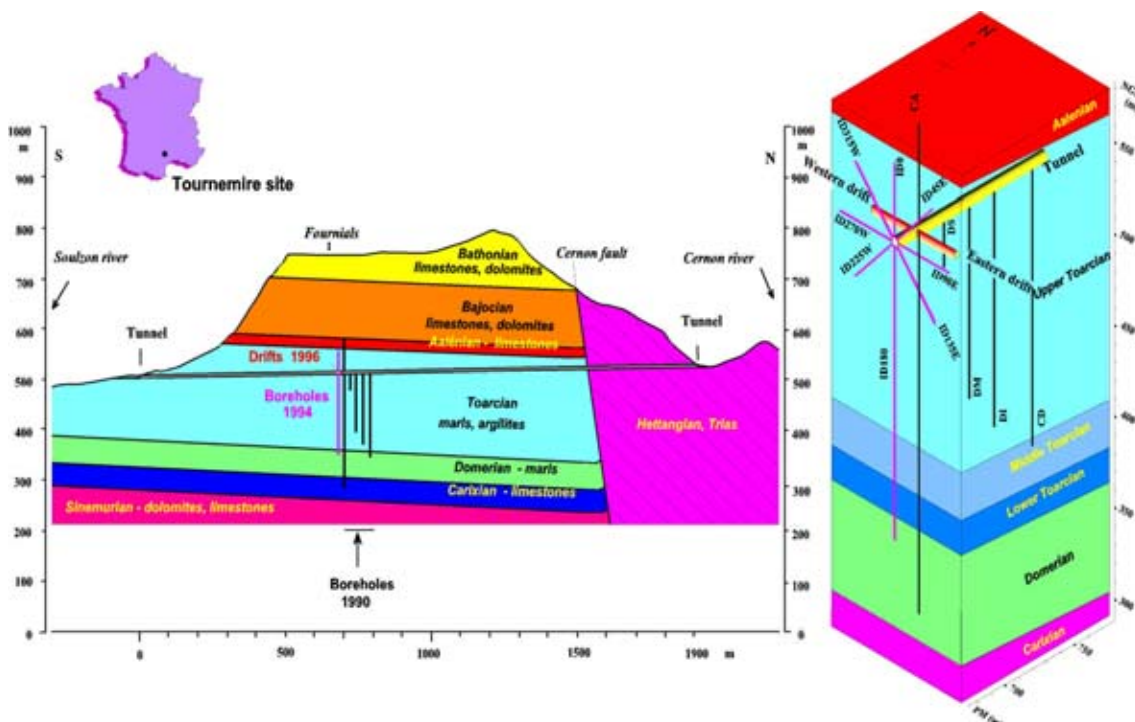


Figure 2.1: Geological cross section and a block showing the main tunnel and boreholes

2.1.1 Geological setting

The Tournemire site is located in a Mesozoic marine basin on the Southern border of the French Central Massif. The sedimentary formations of this basin are characterised by three major layers of Jurassic age (Figure 2.1). The analysed argillaceous formations correspond to a 250 m thick layer located between two limestone and dolomite layers (300 – 500 m thick). The Tournemire site is located in a rock massif with an upper surface at 850 m in elevation, and bounded by two valleys of 450 – 500 m elevation.

The Tournemire argillaceous rocks consist of sub-horizontal argillites and marls belonging to Toarcian and Domerian formations. The Toarcian formation is the thickest series (200 m) composed of argillites and marls. Marls (50 m thick) essentially form the Domerian formation. These formations are located between two limestone aquifers: a regional aquifer in the lower part (Carixien aquifer) and a local aquifer in the upper part (Aalenien aquifer) (Figure 2.1).

2.1.2 Structural and tectonic analyses

The Tournemire site corresponds to a sub-horizontal monoclinial structure of sedimentary Jurassic series affected by a regional E-W striking major Cernon fault (80 km in length) in the northern part (figure 2.1). This fault, which is the major existing discontinuity, has uplifted the limestones and dolomites of the lower series. The structural model consists of an E-W striking block (10 km wide) delimited to the North by the major Cernon fault and to the South by an E-W striking St Affrique – St Jean d’Alcapiès fault (16 km in length).

The Tournemire massif appears affected by some secondary faults of hectometric scale, which are associated with fractured zones. The structures define an unfractured blocks of clay stones and marls limited by the fault zones. Fracture scale ranges from the micro fracture to the fault zone, which is characterised by breccias sheared material. The fractures are generally filled by calcite with occurrence of cubic pyrite in minute amounts. A main fault or fractured zone (roughly 20 m wide) is present in the Western drift intersecting the main tunnel. In contrast, in the Eastern drift only some single fractures are observed (Figure 2.2).

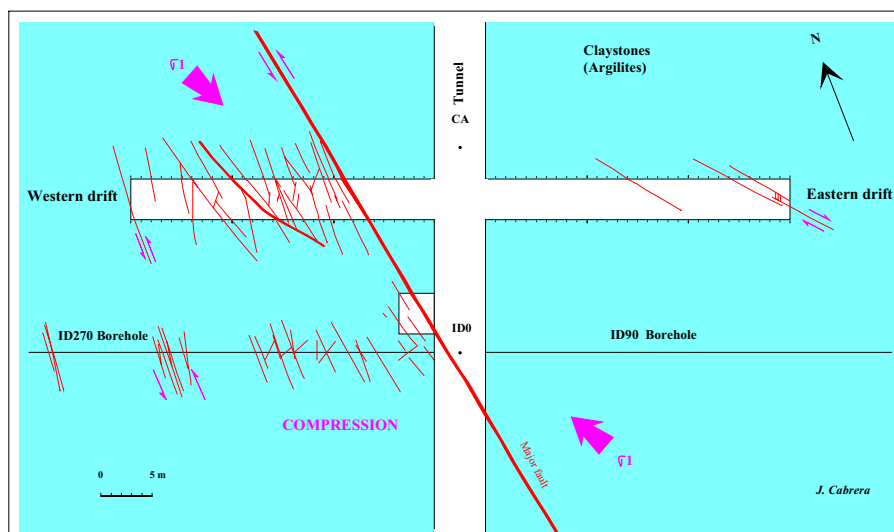


Figure 2.2: Structural and tectonic sketch in the drifts sector of Tournemire site

2.1.3 Characteristics of the argillaceous medium

The argillaceous rock consists of well-compacted argillites and marls formed by lithostatic pressure and diagenetic processes. These indurate series of rock that represent a solid material, are composed of thinly bedded clay minerals that have a typical anisotropic texture. The clay fraction is predominant (40 – 50 % in volume) and made up of illite, kaolonite, chlorite and smectite. Calcite is the predominant carbonate (10 – 30 %) mineral; dolomite and siderite are present in small portions. Quartz occurs as grains (10 – 20 %) and secondary minerals are represented by muscovite, biotite, albite and K-feldspars. Organic matter and framboidal pyrite are widespread in the matrix. The matrix shows very low water content (1 to 5 % by weight) (figure 2.3) and the saturation seems to be around 100 %. The mean total porosity is between 6 and 9 %, and the pore size is extremely small, in the order of 2.5 nm. Grain density is $(2.7 - 2.8) \cdot 10^3 \text{ kg/m}^3$ and specific surface varies between 23 and 29 m^2/s . A large capillary pressure is measured, ranging from 3 to 50 MPa. The cation exchange capacity is about 10 meq/100g and pore water has a moderate salinity (density being 1500 mg/l) with reducing condition and slightly alkaline characteristics.

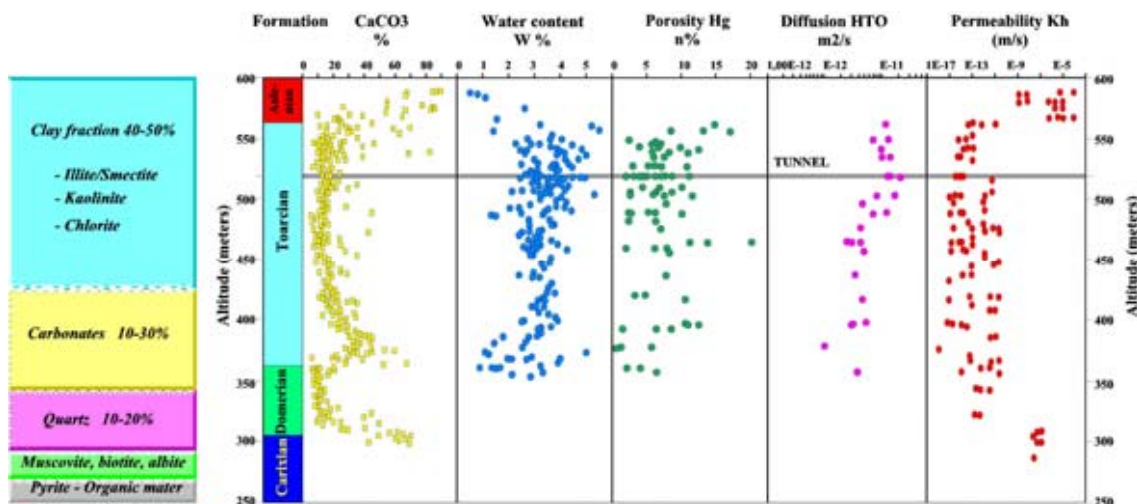


Figure 2.3: Characteristics of argillites and marls of Toarcian and Domerian formations

2.2 Geomechanical characterisation

The argillaceous formations of the Tournemire site is characterised by well-indurated argillites and marls and its mechanical properties are intermediate between those of a plastic clay and crystalline rock. The geomechanical investigations were performed in the laboratory as well as in the field.

2.2.1 In situ stress field

Two complementary series of stress measurements were undertaken, to determine the initial stress field at the Tournemire site. The method used for both series was the HTPF method – Hydraulic Testing of Pre-existing Fractures.

The first test series was conducted in 1995 in a vertical borehole at depths between 41 and 143 m. From this series of tests, it was noted that the stress state in the massif is isotropic in the upper part of the zone tested, with $\sigma_v = \sigma_H = \sigma_h = 4.32 \pm 1.13$ MPa and a direction of N 72° E for the maximum horizontal stress σ_H . This orientation fits poorly with what we know of tectonic stress in the region as a whole (N 160°) (Cabrera et al., 2001).

A second test series was carried out in 1999 in the same area where the first tests were conducted. Near the tunnel, the amplitude and orientation of each of the three local stress field components are as follows:

$\sigma_h = 2.1 \pm 1.0$ MPa, oriented N 072° \pm 15°E and at an angle of 10° to the horizontal;
 $\sigma_v = 3.8 \pm 0.4$ MPa, oriented N 072°E and at an angle of 10° to the vertical;
 $\sigma_H = 4.0 \pm 2.0$ MPa, oriented N 162° \pm 15°E.

The two test series are in good agreement with regard to the amplitudes of the normal stresses on four fractures tested in both surveys, but differ markedly with respect to the orientation of these fractures. The two test series gave two different stress fields in the neighbourhood of the tunnel. The largest difference between the two measured stress fields concerns the directions of principal stress - a difference of 90° for maximum horizontal stress. This difference is not yet explained and no conclusion can be done concerning the correct direction of principal stress.

2.2.2 Mechanical properties

Tournemire argillite displays thinly bedded clay minerals with a typical anisotropic texture which governs strongly its mechanical behaviour. The mechanical behaviour is characterised by using a transversely isotropic material described by the generalised Hooke's law. The five independent elastic parameters have the following values:

$E_1 = 27680 \pm 4040$ MPa and $\nu_{12} = 0.17 \pm 0.03$
 $E_2 = 9270 \pm 4090$ MPa and $\nu_{23} = 0.20 \pm 0.03$
 $G_{12} = 3940 \pm 480$ MPa

where E_1 , E_2 are the Young modulus in the directions parallel to the plane of isotropy and perpendicular to it, respectively; G_{12} is the shear modulus for the plane normal to the plane of isotropy. The Poisson ratio, ν_{ij} characterises the lengthening deformation in the j direction due to the normal stress acting in the i direction.

The uniaxial compressive strength ranges from 13 to 32 MPa and the maximal strength is between 20 and 57 MPa, depending on loading orientation. Moreover, the tensile strength in the direction parallel to the stratification plane is 3.6 MPa.

The Coulomb failure criterion is considered to represent the failure mode of the rock. The main mechanisms of failure are the extension and sliding of the bedding planes in the argillite. The failure surface on the (σ_1 - σ_3) plane gives a friction angle of 20° and cohesion between 6.7 and 10.8 MPa. During the residual phase of the strength testing the material loses its cohesion at 1.4 MPa (Rejeb, 1999).

The triaxial creep tests gave a primary creep with a low strain ranging from 0.02 to 0.1 % under a deviatoric stress of 20 MPa acting for three months. This low time-dependent strain is governed by material anisotropy (Rejeb, 2003).

2.2.3 Hydraulic properties

The Tournemire massif is bounded by two valleys and the present major water circulation in the massif is essentially located in the lower and upper limestones aquifers that bound the argillaceous layer, and along the regional Cernon fault that cuts across the sedimentary series. The regional Carixian lower aquifer and the upper Aalenian aquifer are characterised by a permeability of about 10^{-8} and 10^{-6} m/s, respectively. In contrast, the argillaceous series are characterised by a very low permeability.

The permeability of the argillaceous matrix was measured in laboratory and in situ. The laboratory tests give very small values, ranging between 10^{-11} and 10^{-15} m/s. In situ tests, mainly pulse tests performed in the Toarcian and Domerian formations, give also a very low permeability ranging from 10^{-10} and 10^{-14} m/s.

Pore water pressure is measured around the tunnel by using multi-mini piezometers in some boreholes. These measurements give a low pore water pressure ranging from 2 to 6 bars.

2.2.4 Humidity properties

The Tournemire argillite contains 40% argillaceous minerals, including approximately 10% illite/smectite, making it subject to swelling and contraction in response to desaturation and resaturation processes, like all argillaceous materials. Adsorption isotherms have been obtained for samples in equilibrium with various hygrometries, and measurements of variations in water content and sample volume have been performed. The lower the hygrometry, the lower the water content and argillite volume. The maximum decrease in volume is 1.5%, for a change in relative humidity of 15% (Daupley, 1997). The free swelling pressure measured on the argillaceous samples is 0.5 MPa.

The mechanical behaviour of the rock is also sensitive to its saturation state. Triaxial compressive tests, carried out on the Tournemire argillite samples submitted to suction pressure, show that in dry atmosphere the average values of elastic modulus, the compressive strength and the cohesion are higher; while the Poisson's ratio is lower (Vales et al., 2004).

In the Tournemire site, drying produces capillary pressures of up to 50 MPa, leading to flaking and fissuring of gallery walls and working faces shortly after the end of excavation. These desaturation fractures are nearly horizontal and follow the stratification of the rock material, with rather regular 20 cm spacing. They are closed during summer (humidity around 100%) and they are opened during winter (40% of humidity), (Rejeb et al., 2002).

2.3 EDZ characterisation

2.3.1 EDZ geological mapping

The old tunnel is covered by masonry blocks and this makes it difficult to observe its EDZ. However, the opportunity to observe the EDZ of the tunnel is offered by the excavation of the Eastern and Western drifts in 1996.

The first set of observations is fractures on the wall and on the floor of the 1996 drifts. These fractures are found to be sub vertical or 45 ° oriented, and parallel to the axis of the old tunnel. They are essentially open and partially filled by recent gypsum crystals. They are probably related to stress redistribution caused by the old tunnel excavation. The extension of these fractures is less than 2 m at the entrance of the Eastern drift. The development of the EDZ in the western side of the tunnel is somewhat different, with a less regular development of fractures and a smaller extension of the EDZ. The only apparent difference between the two sides of the tunnel is the presence of a major fault zone observed in the wall of the Western drift in the immediate vicinity of the EDZ from the main tunnel. This hypothesis should be analysed to confirm the link that might exist between the faulted zone and differences in the development of the EDZ on the eastern and western sides of the old tunnel (Fig. 2.4).

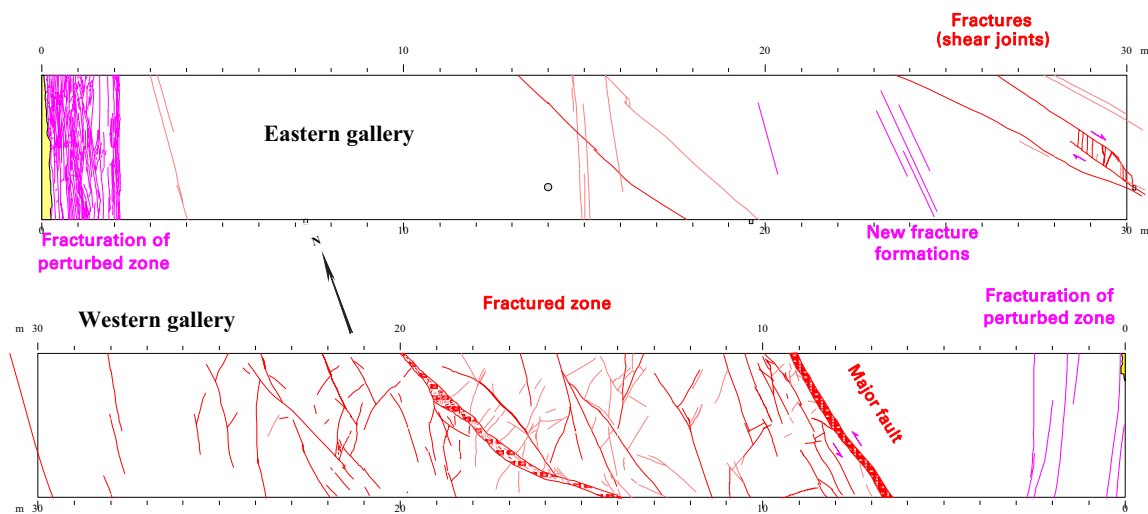


Figure 2.4: Pre-existing tectonic fractures and the EDZ fractures induced by tunnel excavation

Several boreholes have been drilled in the old tunnel and in the 1996 drifts. The geological analysis of the samples extracted from these boreholes allowed observation of the extent of fracturing associated with the EDZ for each excavation. The two drifts exhibit a similar damaged layer with a thickness ranging from 15 to 65 cm. Figure 2.5 summarizes the observations carried out from the radial boreholes of the old tunnel. The extent of the EDZ of the tunnel on this cross-section is deduced from extrapolation of observed fractures on the samples. This EDZ is asymmetrical with respect to the fault plane intersecting this section. The extension of EDZ confirms the observation at the intersection of East /West drifts and the tunnel (Fig. 2.4). Probably, the in situ stresses are locally modified by the presence of the tectonic fault. New radial boreholes, far from tectonic faults, are planned to give a more precise EDZ extent in the tunnel walls.

The excavation of the new drift in 2003, confirmed the first observations done on the intersection of the tunnel and the 1996 drifts. The same vertical fractures with 2 m in extent are associated to the EDZ tunnel. Figure 2.6 gives a general view of the outline of the EDZ developed along the tunnel. This outline is deduced both from interpretation and direct observation of fracturing (boreholes and drifts).

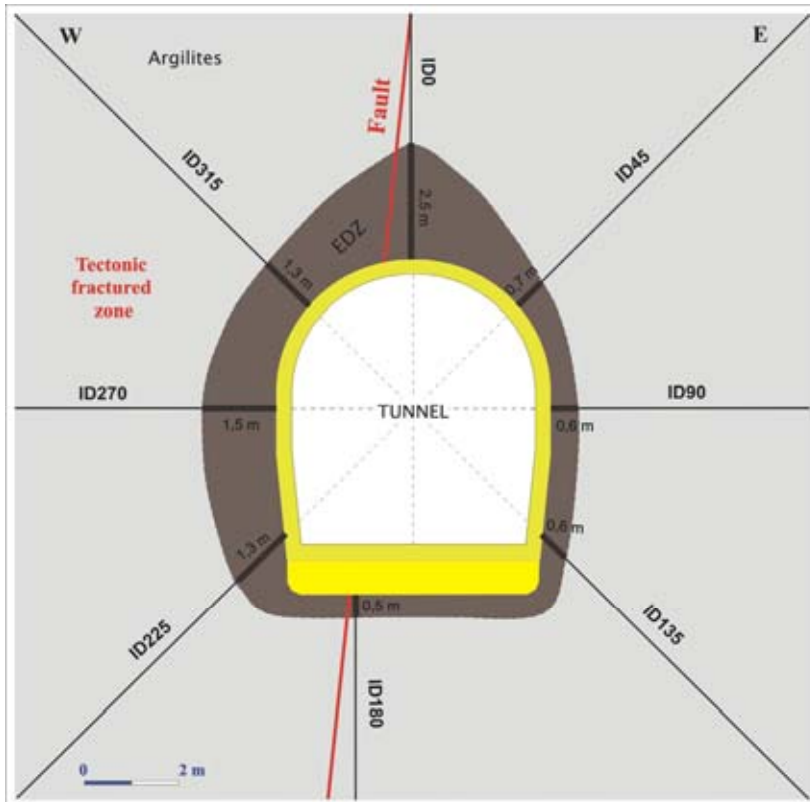


Figure 2.5: The extent of the EDZ around the old tunnel

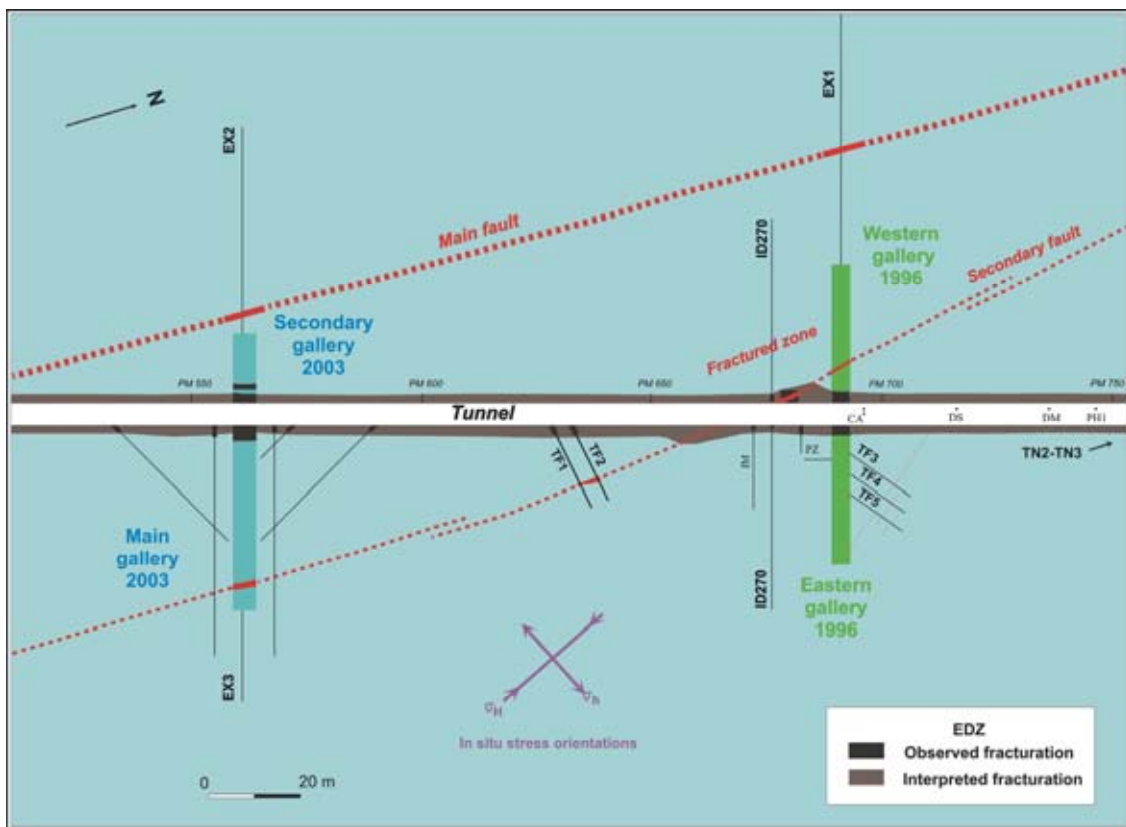


Figure 2.6: Outline of the EDZ developed along the tunnel

2.3.2 EDZ permeability measurements

The hydraulic properties of the EDZ around the tunnel have been assessed by applying successive pulse tests carried out using a small packer interval of 5 cm in the boreholes at up to 6 m from the tunnel walls. These tests show that there is a marked increase in permeability over a distance of 1.50 m from the tunnel wall, with a sharp boundary of the EDZ at that depth. The results of the tests within the Eastern drift suggest that the permeability is enhanced over a distance of approximately 0.50 m, but there is in addition a transition zone of approximately 1 m between the EDZ and the unaffected argillite. The conclusion of this testing is that the permeability increase due to the presence of the EDZ and appears to be 5 to 6 orders of magnitude higher than in the virgin rock.

2.4 Definition of Task C

By taking into account of the initial in situ stress field and the mechanical compressive strength derived from laboratory tests, calculations have shown that it is not likely to have a failure after the excavation of the old tunnel. This conclusion means that the simple mechanical analysis cannot explain the development of the EDZ around the tunnel. Therefore, some physical phenomena like time-dependent behaviour of the Tournemire argillite, coupled hydro-mechanical processes and damage mechanism, should be taken into account in understanding and modelling EDZ development.

The objectives of Task C are to study the physical phenomena involved in excavation in the argillaceous rock, to develop and apply adequate numerical codes to model these phenomena, and to compare alternative modelling approaches. These objectives can be reached since the Tournemire site provides an extensive and sound database obtained both from laboratory tests and in situ investigations. This makes possible the comparison between numerical predictions and in situ data especially on the EDZ extent and its evolution with time. To achieve these objectives, Task C is divided into three subtasks:

Task C1: Modelling the EDZ around the tunnel

The first step concerns the understanding of the EDZ development around the old tunnel. The failure mechanism should be identified by analysing the in situ stress field and the orientation of the bedding planes with respect to the axis of the tunnel and the degree of anisotropy. Therefore, numerical models will be developed to predict the extent of the EDZ around the tunnel. The results of calculations using various approaches should be compared with measured data in order to validate the computer models used in the simulations.

Task C2: Evolution of the EDZ in time

In this step, we should include the effect of time on the EDZ development. At the Tournemire site, we have three openings excavated at three different times. The intention is to assess the EDZ of the one century old tunnel, the EDZ of the ten years old drifts (1996) and the EDZ of the three years old drifts (2003). The numerical predictions will be compared with the extent of the EDZ measured at a given time for these three excavations. The calibration phase followed the simulations will be useful to predict the evolution of the EDZ with time.

Task C3: Effect of the fracture zone on the extension of the EDZ

Figure 2.4 shows that the nature of the EDZ around the old tunnel is asymmetric. It is probably due to the tectonic fracture zone in the Western drift (figure 2.2). Performing calculations where the fractured zone is included in the simulations can possibly explain this observation.

2.5 Detail description of Task C1

The main objective of this first subtask is to understand the origin of the EDZ developed around the old tunnel at the Tournemire site.

The research teams are asked to prepare a numerical model of the host rock near the tunnel and to predict the extent of the EDZ around the tunnel. The definition of EDZ that is considered in this task is equivalent to the failure zone around the tunnel. The comparison between numerical results and the in situ observations should be done in order to validate the approach and to understand the EDZ development around the tunnel.

2.5.1 Modelling data

The Tournemire tunnel is built in argillaceous rock and lined with calcareous masonry on the walls. The floor of the tunnel is founded on ballast, covered with wood and concrete. The main profile and the dimensions of the tunnel are presented in Figure 2.7.

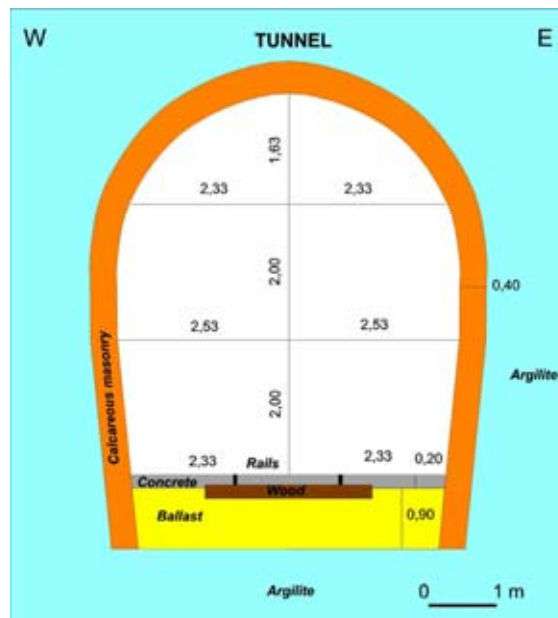


Figure 2.7: Profile and dimensions of the old tunnel

The material properties are summarised as below.

Argillite:

$E_1 = 27680 \pm 4040$ MPa and $\nu_1 = 0.17 \pm 0.03$;

$E_2 = 9270 \pm 4090$ MPa and $\nu_2 = 0.20 \pm 0.03$;

$G_{12} = 3940 \pm 480$ Mpa;

$13 \text{ MPa} < R_c < 32 \text{ MPa}$ and $R_t \approx 3.6$ Mpa;

Mohr Coulomb failure criteria: Friction angle $\phi = 20^\circ$;

Cohesion (depending on the orientation): $C(\theta) = 10.8 \cos^2 \theta + 9.3 \sin^2 \theta - 13.5 \sin^2 \theta \cos^2 \theta$;

Permeability values: $10^{-15} \text{ m/s} \leq K \leq 10^{-11} \text{ m/s}$ (laboratory tests) and $10^{-14} \text{ m/s} \leq K \leq 10^{-10} \text{ m/s}$ (in situ tests).

Other materials:

Calcareous masonry: $\rho = 25 \text{ kN/m}^3$ and $E = 20 \text{ GPa}$;

Ballast: $\rho = 20 \text{ kN/m}^3$ and $E = 500 \text{ MPa}$.

Concerning the initial conditions, note that according to uncertainties in the results of the stress measurements, the research teams may use the two possible stress field given below:

- 1) $\sigma_v = \sigma_H = \sigma_h = 4.32 \pm 1.13 \text{ MPa}$ and a direction of N 72° for stress σ_H
- 2) $\sigma_h = 2.1 \pm 1.0 \text{ MPa}$, oriented N $072^\circ \pm 15^\circ \text{E}$ and at an angle of 10° to the horizontal;
 $\sigma_v = 3.8 \pm 0.4 \text{ MPa}$, oriented N 072°E and at an angle of 10° to the vertical;
 $\sigma_H = 4.0 \pm 2.0 \text{ MPa}$, oriented N $162^\circ \pm 15^\circ \text{E}$.
- 3) In situ pore pressure: $P_o \approx 5 \text{ bars}$

Specific boundary conditions: the tunnel was excavated manually in 1881 and the history of the excavation is unknown.

2.5.2 Required results

- Full details of the construction of the model and calculations performed.
- Displacement and stress fields around the tunnel 100 years after construction (contour zones, profiles).
- Extent of the EDZ around the tunnel 100 years after construction.

3 EDZ modelling by CEA/IRSN team

3.1 Introduction

The CEA/IRSN team's contribution to Task C1 includes three calculations: a pure mechanical calculation (M), a coupled hydro-mechanical calculation (HM) assuming saturated rocks, and coupled hydro-mechanical calculation assuming unsaturated rock (HMU) (Millard and Rejeb, 2005). In all cases, the EDZ around the tunnel has been estimated on the basis of a post-processing of stress calculations, using a Mohr-Coulomb failure criterion. These calculations are performed by using the CEA finite element code CASTEM, which can simulate fully coupled THM processes (Verpeaux et al., 1989).

3.2 Data and assumptions

3.2.1 Geometry and mesh

The geometrical data have been taken as defined in the task specifications (figure 2.7). Because of the extent of the tunnel, a two-dimensional analysis is performed, under the assumption of plane strain. The size of the considered domain is 80m x 80m, the tunnel being placed at the centre of the model.

The various calculations do not require the same refinement of the model mesh. For this reason two different meshes have been used. The first mesh, used for M and coupled H-M calculations contains 11036 nodes and 3560 quadratic elements. For the second mesh, which is more refined and used for the HMU calculation, the total number of nodes is 25106 and the total number of quadratic elements is 8458. The ballast, the concrete and the calcareous masonry on the tunnel walls have not been considered in this analysis.

3.2.2 Initial conditions

Before excavation of the tunnel, the rock mass is supposed to be in an homogeneous state of stresses, defined according to the specifications: $\sigma_v = 3.8$ MPa, $\sigma_h = 2.1$ MPa and $\sigma_H = 4.0$ MPa. The initial pore pressure is supposed to be uniform, equal to $P_0 = 0.5$ MPa, and the argillite is supposed to be in a saturated state. The initial porosity of the argillite is $\phi_0 = 0.075$.

3.2.3 Boundary conditions

Concerning the mechanical boundary conditions, constant in situ stresses are applied on the top and lateral boundaries of the model. At the bottom, the vertical displacement is set to zero. During excavation (15 days), the stress vector applied on the tunnel wall is linearly decreased from its virgin value to zero at full excavation.

For the H-M calculation, in addition, the fluid pressure is maintained at its initial value on the external boundary of the domain, whereas inside the tunnel, it is decreased to zero during the excavation phase.

Finally, for the HMU calculation, the only difference, compared to the H-M case, concerns the fluid pressure boundary condition inside the tunnel. Indeed, the annual periodic variations of the temperature and relative humidity in the tunnel have been taken into account. From the in situ recorded measurements (Rejeb and Cabrera, 2004), a sinusoidal idealization has been used, with the following mean values and variance:

Temperature: $10^{\circ} \pm 5^{\circ}$ and
Relative humidity: $70\% \pm 30\%$.

From these variations, the corresponding water pressure is derived according to Kelvin's law, assuming a constant atmospheric gas pressure. In the calculation, it was assumed that at the end of the excavation, the temperature and the relative humidity were at their mean value respectively, and that a cooling period was starting, corresponding to a decrease in temperature as well as in relative humidity. The time history of the liquid pressure at the tunnel wall, over one year after excavation, is shown on Figure 3.1.

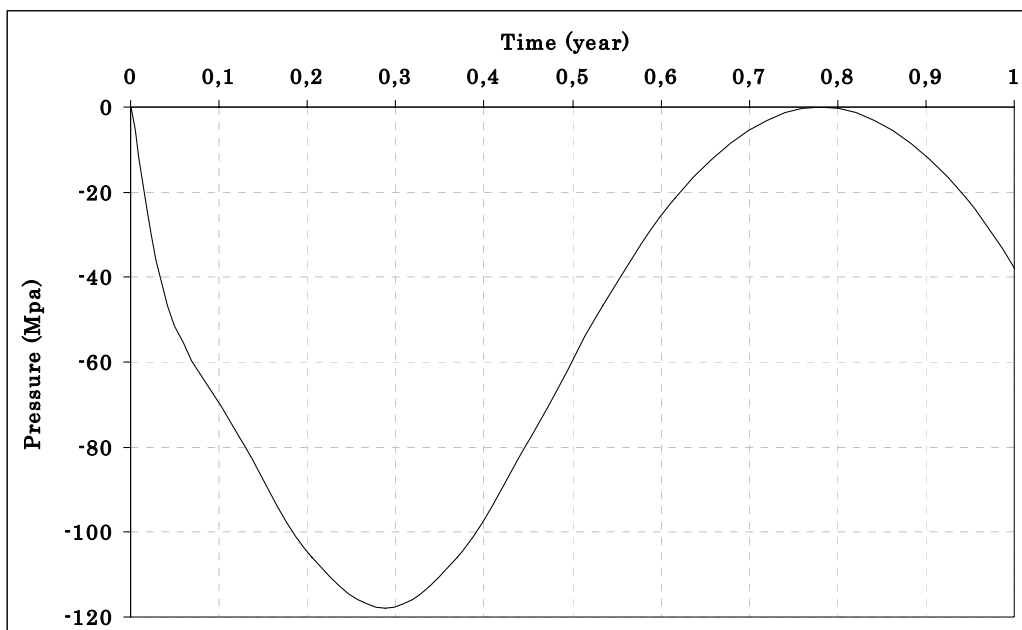


Figure 3.1: Time history of the pressure in the tunnel, over one year after excavation

3.2.4 Material properties

The anisotropic mechanical parameters of argillite given in section 2.5.1 are used in the M and HM calculations. In the HMU calculation (where U indicates unsaturated case), it was only possible to use an isotropic elastic material model. The corresponding Young's modulus and Poisson's coefficient were chosen as: $E = 27680$ MPa and $\nu = 0.2$.

For the saturated HM calculation, the following isotropic properties of the argillite have been selected (anisotropic properties were not available):

Biot's coefficient : $b = 0.75$
 Biot's modulus: $M = 5.26 \cdot 10^{10} \text{ Pa}$
 Intrinsic permeability: $K = 10^{-19} \text{ m}^2$

For the unsaturated H-M calculation, in addition, the capillary pressure curve as well as the relative permeability must be given. Both quantities have been assumed to follow a Van Genuchten model with the following expression:

$$P_c(S_l) = M [S_l^{-1/m} - 1]^{1-m}, \text{ with } 0 < m < 1$$

$$k_{rl}(S_l) = S_l^{1/2} [1 - (1 - S_l^{1/m})^m]^2$$

where S_l represents the liquid saturation, and M and m are two constants. They have been calibrated from experimental data reported by Ramambasoa (2001) by means of a least squares fitting technique. The adopted values are: $M = 10.65 \text{ MPa}$ and $m = 0.426$. The corresponding capillary pressure curve is displayed in Figure 3.2.

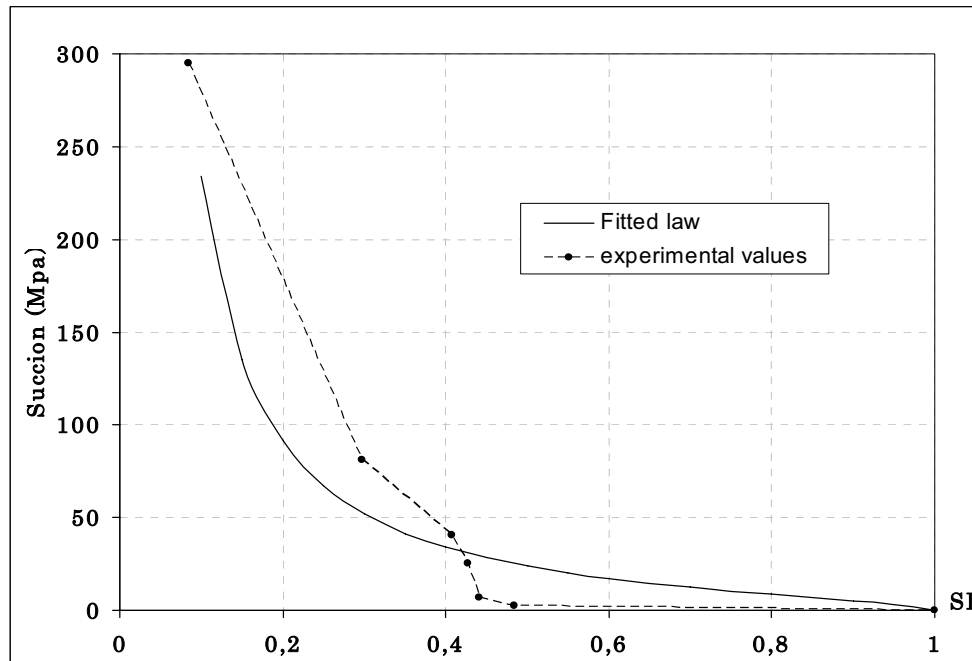


Figure 3.2: Capillary pressure curve fitted from laboratory measurements

In all the cases, the EDZ extent has been evaluated on the basis of a post-processing treatment of the stress state, according to a Mohr-Coulomb failure criterion. When the criterion results' in negative values, the state of stresses lies within the elastic domain. On the contrary, when the criterion is positive, the argillite is considered to be damaged. In the present application, the cohesion has been taken equal to the residual cohesion of the argillite, that is $C = 1.4 \text{ MPa}$, and the friction angle $\phi = 20^\circ$.

For the HM and HMU calculations, the stresses used for post-processing of failure are the effective stresses. In both cases, they are defined by: $d\sigma' = d\sigma + b S_l dp_l$ (where S_l is equal to 1 in the saturated case and b is the Biot's constant). Note that the choice of effective stresses is not coherent with the use of the rock mass data that were derived mostly from undrained laboratory tests (short duration).

3.3 Mechanical calculations

For a given time, the space evolution of various quantities (displacement, stresses, failure) has been plotted along two profiles: a horizontal profile, labelled LH1, and a vertical one, labelled LV2 (Figure 3.3). The evolution of failure according to the failure criterion along the two profiles is shown in Figures 3.4 and 3.5. As can be expected, the tunnel excavation leads to an increase of deviatoric stress close to the tunnel wall. As a consequence, a higher value of the Mohr Coulomb failure stress is obtained in this zone.

LV2

Figure 3.3: Profiles selected for result display

LH1

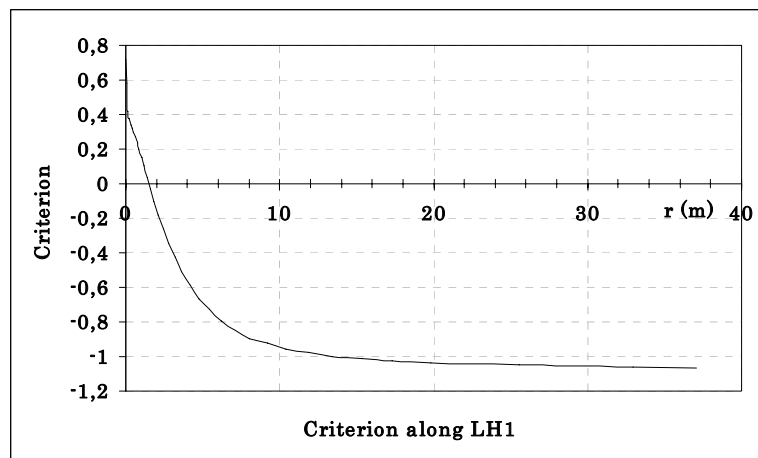


Figure 3.4: Mohr Coulomb failure criterion after excavation along profile LH1

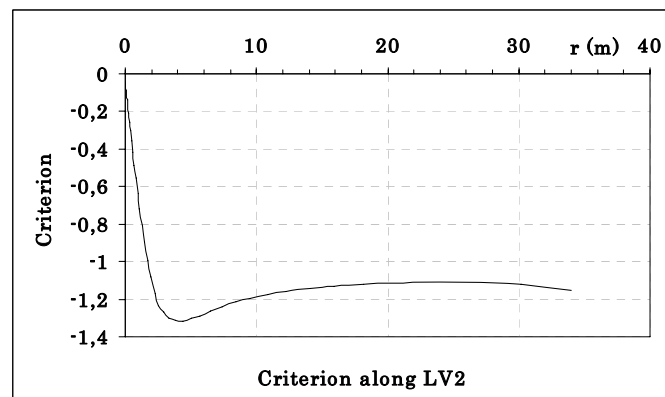


Figure 3.5: Mohr Coulomb failure criterion after excavation along profile LV2

Due to the anisotropy of the initial stress field, the results indicate that in the horizontal direction, a damaged zone is expected, while there is no damage in the roof of the tunnel. Figure 3.6 shows the plot of the EDZ (zone where the criterion is positive) for the case of anisotropic initial stress state. Along profile LH1, the width of the EDZ is about 1.5 m.

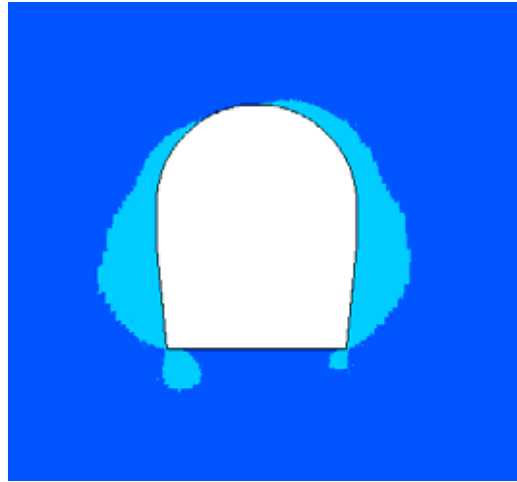


Figure 3.6: Extent of the EDZ after excavation for anisotropic initial stresses

Again, this result is largely due to the anisotropy of the initial state of stresses. For comparison, another purely mechanical calculation has been performed, called improperly hereafter the ‘isotropic initial stresses’, with the same data except for the initial state of stresses, which was taken as: $\sigma_v = \sigma_H = 3.0$ MPa with σ_h unchanged at 4.0 MPa. In this case the extent of the EDZ is presented in Figure 3.7, showing a more uniform distribution of the EDZ around the tunnel. The anisotropy of the initial state of stresses has much more influence on the results than the anisotropic elastic properties.

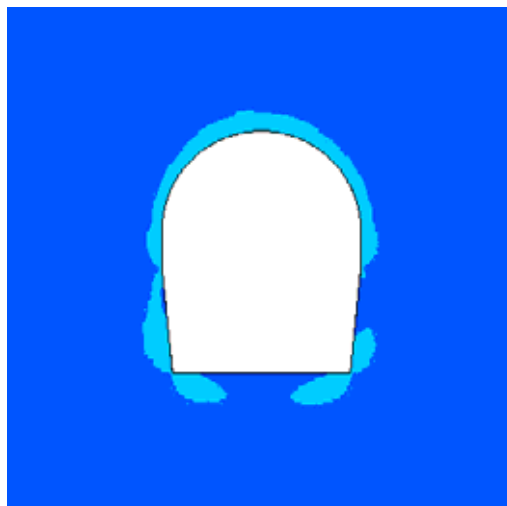


Figure 3.7: Extent of the EDZ after excavation for ‘isotropic’ initial stress state

All the above results have been obtained on the basis of the residual cohesion $C = 1.4$ MPa. For a higher value of the cohesion, such as the intact rock one, varying between 6.7 MPa and 10.8 MPa, no damage is predicted by the mechanical calculation.

3.4 Hydro-mechanical calculations with saturated conditions

Contrary to the previous mechanical calculation, the hydro-mechanical response in a saturated rock mass excavation is a transient phenomenon. Therefore, calculation has been performed for a period of 10 years following the start of excavation.

In order to visualize the evolution with time of the various responses, they have been plotted on the same figure immediately after excavation (time 0), one year and ten years after excavation, respectively.

The histories of pressure along profiles LH1 and LV2 are respectively shown in Figures 3.8 and 3.9. Along the horizontal profile, the excavation induces a large increase of the pressure, with reference to its initial uniform value. This is accompanied by a large decrease along the vertical direction, leading to negative values (close to - 2 MPa). These variations are directly correlated with the trace of the strain tensor, which is negative on the lateral walls of the tunnel (thus inducing an increase of pressure) and positive at the top and bottom of the tunnel (thus inducing a pressure decrease). As time proceeds, the pressure profiles tend to smoothen to reach the asymptotic steady state regime, corresponding to a hydrostatic equilibrium between the zero value at the tunnel wall and the far field value of 0.5 MPa at the outer boundary.

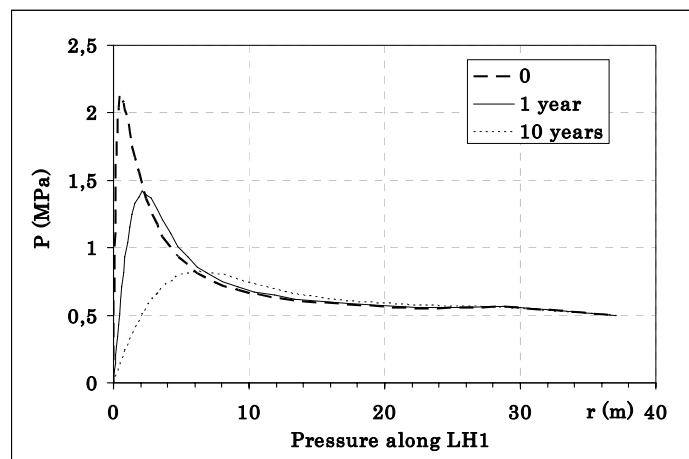


Figure 3.8: Profiles of liquid pressure along profile LH1

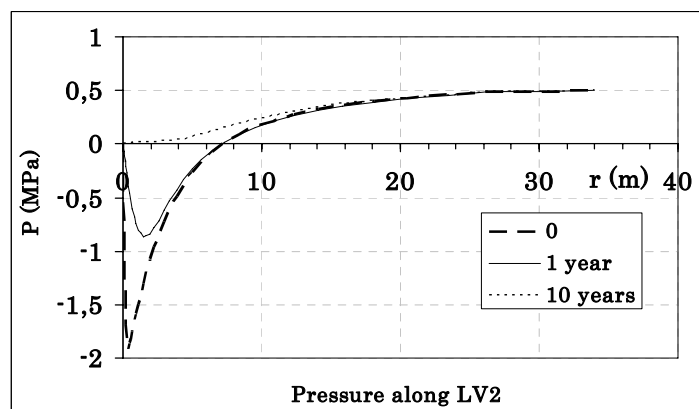


Figure 3.9: Profiles of liquid pressure along profile LV2

The change of total stress along the profiles for the total stresses can be compared to the pure mechanical results; particularly the radial stresses that are also nearly constant with time. This is probably because these stresses are principally statically determined by the boundary conditions. The other components of stresses show a rapid variation close to the tunnel wall, and tend to vanish with time. This variation is due to the transient response of the porous medium, for which the rock mass loading induced by the excavation is supported by both the skeleton and the fluid, and this effect is more pronounced in the horizontal direction than in the vertical one.

The failure criterion is expressed in terms of effective stresses. The application of the formula: $\sigma' = \sigma + b p_1$ for the radial stress leads to a result showing a rapid variation close to the tunnel wall (in fact the variation of pressure), whereas the two other components show a result similar to the mechanical ones, but with a larger stress magnitude since p is positive.

Generally speaking, at location where p is positive in the model, the effect of p on the stresses will be a translation of the Mohr's circles towards the traction stresses, which brings the stresses closer to the failure limit. In fact, as shown in Fig. 3.10, high values of the Mohr Coulomb criterion along profile LH1 are obtained on a larger width than for the mechanical case. This width decreases as the pressure peak vanishes. This effect is not visible on the vertical profile LV2 (Fig. 3.11), since the pressure algebraically decreases, which moves the effective stress state farther from the failure limit.

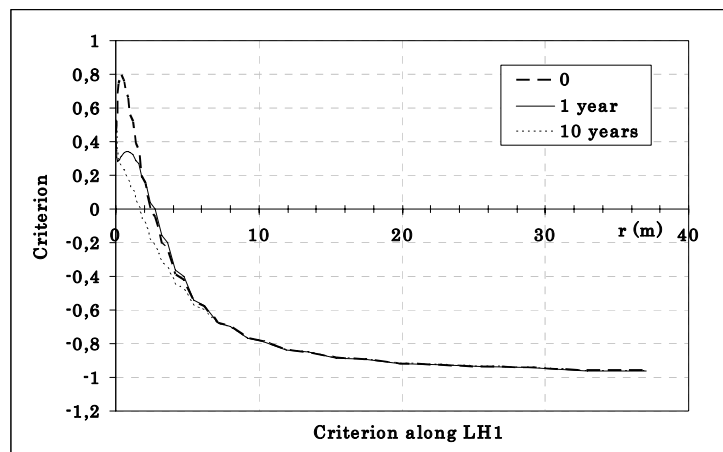


Figure 3.10: Mohr-coulomb failure criterion along LH1

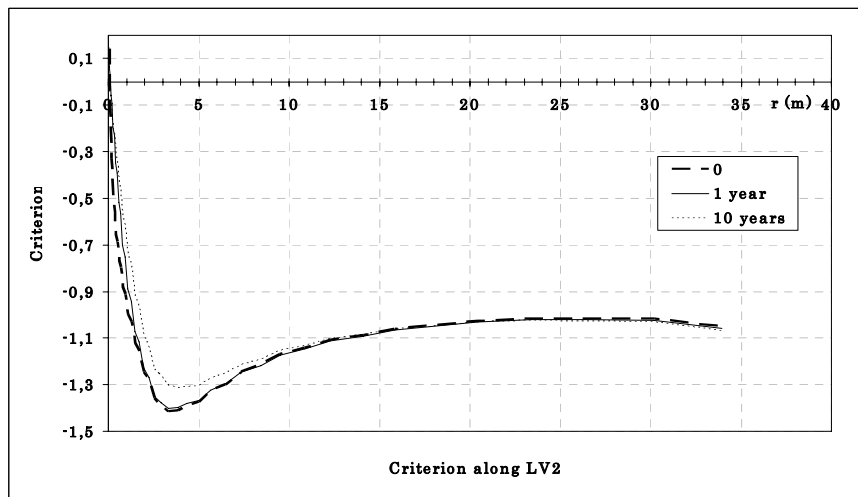


Figure 3.11: Mohr-coulomb failure criterion along LV2

Finally, the extent of the EDZ reaches a maximum during the first 6 months following the excavation, reaching a size of about 2.8 m along profile LH1, and then tends to reduce. It must be noticed that this is not realistic, but is due to the fact that the EDZ is estimated by post-processing. The EDZ at the end of excavation is presented in Figure 3.12, and can be compared to the results of pure mechanical (M) calculations as presented in Figure 3.6.

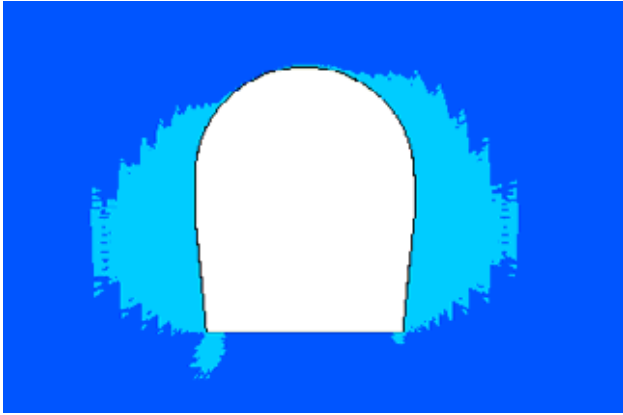


Figure 3.12: Extent of the EDZ after excavation for the case of hydro-mechanical calculations with saturated conditions

3.5 Hydro-mechanical calculations with unsaturated conditions

The hydro-mechanical calculation for unsaturated conditions is more realistic than the two previous ones since the calculations take into account the effect of temperature and relative humidity in the tunnel. The results presented here concern only the first year following the excavation. Of course, some progressive evolution of the damage due to the repeated annual climate cycles is expected. Nevertheless, it is interesting to look first at the effect of the excavation for one cycle of the low relative humidity existing in the tunnel during winter.

The history of pressure along profile LH1 and LV2 are shown in Figs 3.13 and 3.14. Due to the very low permeability and the prescribed relative humidity in the tunnel, the pressure is nearly uniform in the argillite one year after excavation, and exhibits a very sharp gradient in the first 20 cm at the tunnel wall. As can be expected, the saturation shows a similar profile.

Contrary to the mechanical (M) and saturated coupled HM cases, high positive total stresses develop at the tunnel wall in the ‘orthoradial’ and axial directions. In the ‘radial’ direction, the total stress does not change much for the same reason as already stated.

For the effective stresses calculated as explained before, the tendency is reversed: the addition of the pressure effect produces a very large negative ‘radial’ stress, while the two other components decrease from their high positive value to a negative value of the order of magnitude as the initial value. Therefore, a high deviatoric state of effective stress is created at the wall of the tunnel, which will lead to failure. This is visible on the plots of the Mohr-Coulomb criterion in Fig. 3.15. Along profile LH1, the failure is predicted right at the tunnel wall. Farther away from the wall, a narrow intact zone precedes a second damaged zone, which shows similarities with the ones obtained in the other calculations. The thickness of this zone is about 1.5 m and it diminishes with time.

Along profile LV2 (Fig. 3.16), only the wall damage is predicted, which is consistent with the other results.

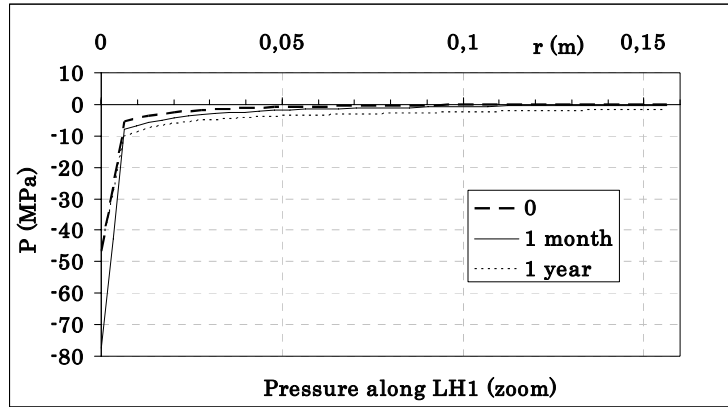


Figure 3.13: Profiles of liquid pressure along LH1; zoom around the tunnel

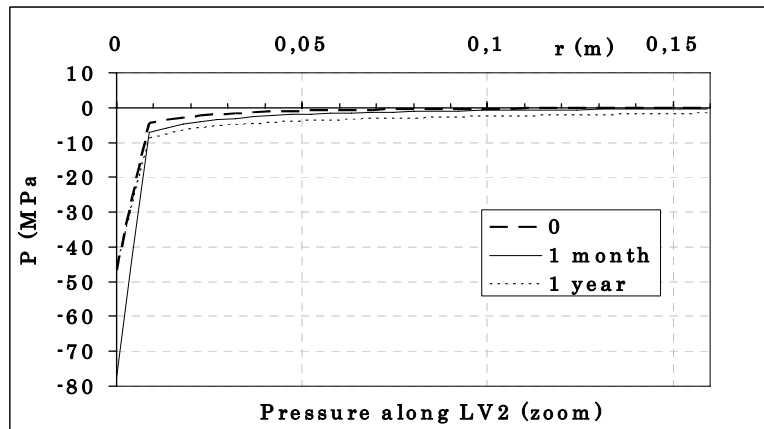


Figure 3.14: Profiles of liquid pressure along LV2; zoom around the tunnel

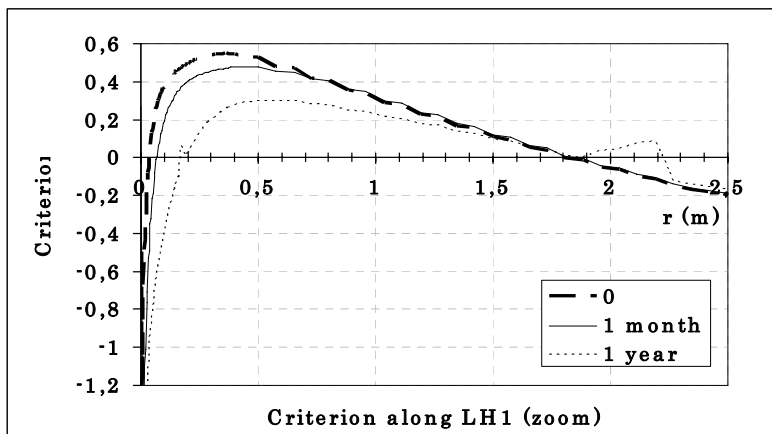


Figure 3.15: Mohr-coulomb criterion along profile LH1; zoom around the tunnel

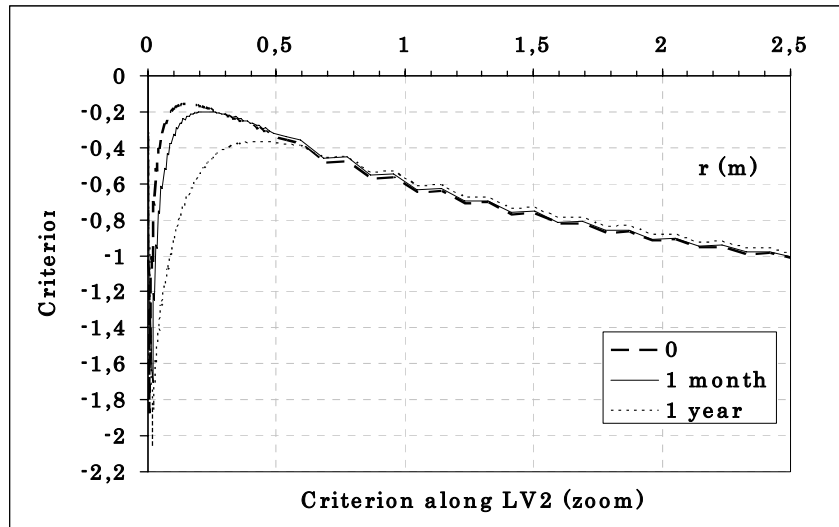


Figure 3.16: Mohr-coulomb criterion along profile LV2; zoom around the tunnel

Finally, the extent of the EDZ evolves slightly due to the environmental conditions during the annual cycle. Figure 3.17 shows the extent of the EDZ, just after excavation, and 1 year after excavation. It can be observed that the EDZ width is slightly reduced, in particular at the upper part of the tunnel. The narrow intact zone around the tunnel has increased. Additional cycles of computation are needed to appraise the trend of the evolution over a century.

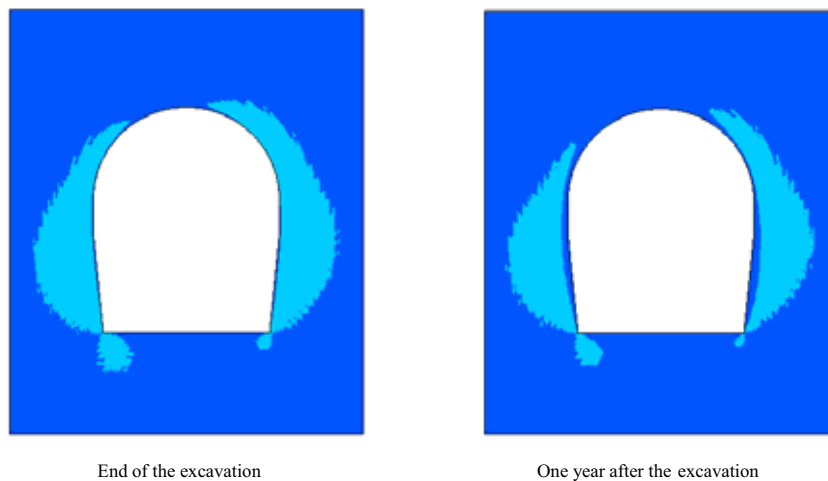


Figure 3.17: Extent of the EDZ just after excavation and one year after excavation

3.6 Synthesis

To study instantaneous response of the argillite to tunnelling, elastic calculations followed by post-processing using Mohr Coulomb failure criterion were performed. To investigate the possible EDZ development over time, hydro-mechanical analyses were performed assuming saturated and unsaturated conditions. These elastic calculations have predicted more or less similar EDZ, despite of the different assumptions regarding the influence of the water in the rock mass or the humidity in the tunnel. From the

results it seems that the initial state of stresses has a major influence on the outcome of the predictions.

All the calculations show that one can only predict an EDZ around the tunnel if lower mechanical rock properties than measured in laboratory are assumed. However, none of the predictions are able to reproduce the shape and the real extent of the observed EDZ in the tunnel.

The evaluation of the EDZ by a simple post-processing technique does not account for the irreversible effect of damage on the mechanical as well as hydraulic behaviour of the argillite. The next step of modelling will consist of a more realistic representation of the argillite behaviour, including time effects such as visco-elasticity and the use of non-linear damage behaviour laws and material models.

4 EDZ modelling by ISEB/BGR team

4.1 Introduction

The driving force of the observed development of EDZ in the Tournemire site may be composed of several processes. Therefore, the aim of this work by the ISEB/BGR team is to identify those processes or coupling effects which might be most responsible for the observed EDZ development. In order to identify the causal connections, a research programme composed by four steps is developed:

- Step 1:** Influence of saturation.
- Step 2:** Influence of anisotropy.
- Step 3:** Influence of plastic or creep effects.
- Step 4:** Influence of fractured zones and fracturing.

This section summarizes the step 1 results of the ISEB/BGR team (Ziefle et al., 2005).

The main hydro-mechanical processes concerning the saturation effects are illustrated in Figure 4.1. A change of saturation over time leads to swelling or shrinking of the material. Additionally elastic or plastic deformations may take place. Both of them, swelling/shrinking and deformations will lead to a change of porosity. Consequently, a change of permeability and pore water pressure (effecting capillary effects and two-phase-flow) will occur.

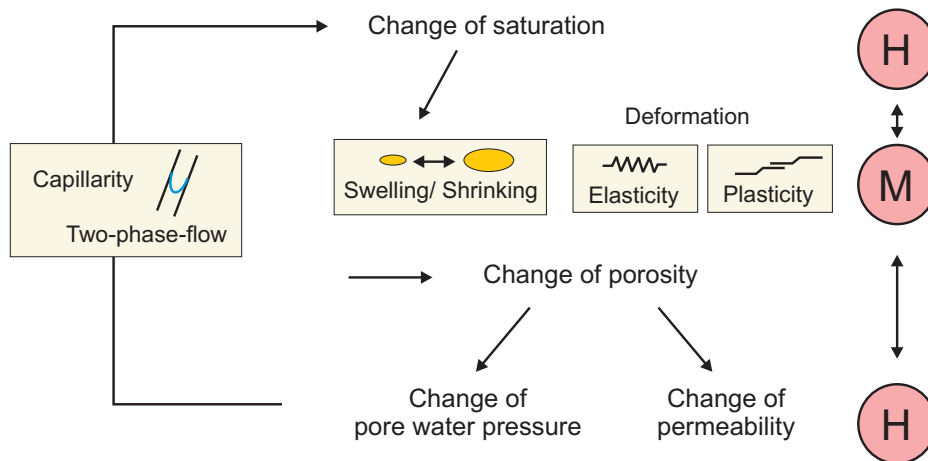


Figure 4.1: Influence of processes on material properties

4.2 Governing equations

Within the Task C investigations, the finite element code Rock Flow is exchange. The ongoing development focuses on the coupled hydro-mechanical processes in argillite.

Coupled hydro-mechanical problems can be divided in separate but coupled sub-problems. For each of these problems balance equations have to be specified. Combined

with constitutive equations (like material laws) a system of equations is built. Within the finite element program this system of equations are solved numerically.

The fundamental equations can be split into the balance equations and the constitutive equations. While the balance equations, like conservation of linear momentum or mass, are solved for every problem, the constitutive equations incorporate the special properties of the problem (e.g. material properties), as presented in the following sections.

4.2.1 Linear swelling model

In order to incorporate swelling or shrinking of the argillite, the Biot consolidation theory is used.

$$\boldsymbol{\sigma}_{\text{tot}} = \boldsymbol{\sigma}_{\text{eff}} - \mathbf{1}\alpha p S^w \quad (4.1)$$

with the effective stress $\boldsymbol{\sigma}_{\text{eff}}$, the total stress $\boldsymbol{\sigma}_{\text{tot}}$, the Biot coefficient α , the water saturation S^w and the pore water pressure p . As a first approximation we assume $\alpha = 0$.

The calculation of total stresses for the elastic case remains

$$\boldsymbol{\sigma}_{\text{eff}} = \mathbf{C} : \boldsymbol{\varepsilon} \quad (4.2)$$

with the fourth-order tensor comprised of the linear elastic coefficients \mathbf{C} and the strains $\boldsymbol{\varepsilon}$ resulting in

$$\boldsymbol{\varepsilon} = \boldsymbol{\varepsilon}^{\text{el}} + \boldsymbol{\varepsilon}^{\text{sw}} \quad (4.3)$$

whereas

$$\boldsymbol{\varepsilon}^{\text{sw}} = \mathbf{1}\beta_{\text{sw}}\Delta S_w \quad (4.4)$$

$$\Delta S_w = S_w^* - S_w^0 \quad (4.5)$$

where S_w^0 is the reference saturation, belonging to the reference volumetric strain $\varepsilon_{\text{vol,sw}}^0$. S_w^* equals the actual saturation, while it is in the range between S_w^{min} and S_w^{max} . Out of this range, the marginal values have to be used (see Figure 4.2).

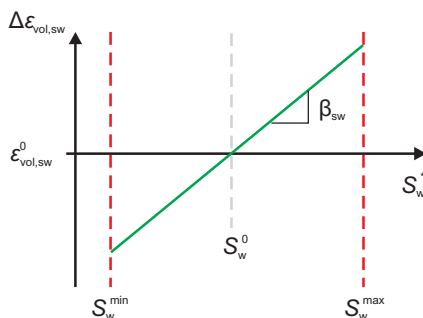


Figure 4.2: Linear swelling model

For this model, the following parameters are given in Table 4.1.

Table 4.1: Material parameters of the linear swelling model of argillite

Material parameter	Value	Unit
Volumetric swelling coefficient, β_{sw}	0.04	-
Swelling model domain:		
Maximum water saturation, S_w^{\max}	1.0	-
Minimum water saturation, S_w^{\min}	0.1	-
Reference water saturation, S_w^0	1.0	-
Volumetric reference strain, $\varepsilon_{vol,sw}^0$	0.0	-

4.2.2 Change of porosity

The updated porosity n is calculated depending on the volumetric strain caused by deformation and/or swelling/shrinking of the material. In this context the volumetric strain caused by deformation ε_{vol} is defined by

$$\varepsilon_{vol} = \varepsilon_{xx} + \varepsilon_{yy} + \varepsilon_{zz}. \quad (4.6)$$

The volumetric strain caused by swelling/shrinking $\varepsilon_{vol,sw}$ is given by

$$\varepsilon_{vol,sw} = \varepsilon_{xx,sw} + \varepsilon_{yy,sw} + \varepsilon_{zz,sw}. \quad (4.7)$$

The following cases can be defined:

Deformation:

The volumetric strain caused by deformation is assumed to affect the pore space, not the size of particles. Consequently, expansion will lead to an increase and compression to a decrease of pore space. The updated porosity is given by

$$n = n_0 + \varepsilon_{vol}. \quad (4.8)$$

Swelling/Shrinking:

Swelling or shrinking leads to a change of the particle size of the argillites. Thus the pore space will decrease during swelling and increase during shrinking

$$n = n_0 - \varepsilon_{vol,sw}. \quad (4.9)$$

Deformation and Swelling/Shrinking:

Consideration of both deformation and swelling or shrinkage effects will lead to the following equation for porosity:

$$n = n_0 + \varepsilon_{vol} - \varepsilon_{vol,sw}. \quad (4.10)$$

4.3 Material properties

The chosen initial material properties for the first calculations are given in Table 4.2.

Table 4.2: Initial material parameters for all cases

Material parameter		Value	Unit
Argillite	Intrinsic permeability, k_i	1.0×10^{-18}	m^2
	Porosity, n_0	0.05	-
	Young's modulus, E	15000	MPa
	Poisson parameter, ν	0.19	-
Water	Density, ρ_w	1000	kg/m^3

The capillary pressure as well as the relative permeability for different saturations has been adapted to the curves given by (Millard and Rejeb, 2005). They are shown in Figure 4.3 and given by the following mathematical expressions

$$p_{c(S)} = M \left[S^{(-1/m)} - 1 \right]^{(1-m)} \quad (4.11)$$

$$k_{(S)} = S^{(1/2)} \left[1 - \left(1 - S^{(1/m)} \right)^m \right]^2 \quad (4.12)$$

where $M = 10.65$ MPa and $m = 0.426$, respectively.

The swelling or shrinking of the argillite causes a change of porosity. The interrelationship of porosity and permeability is assumed to be linear (Table 4.3).

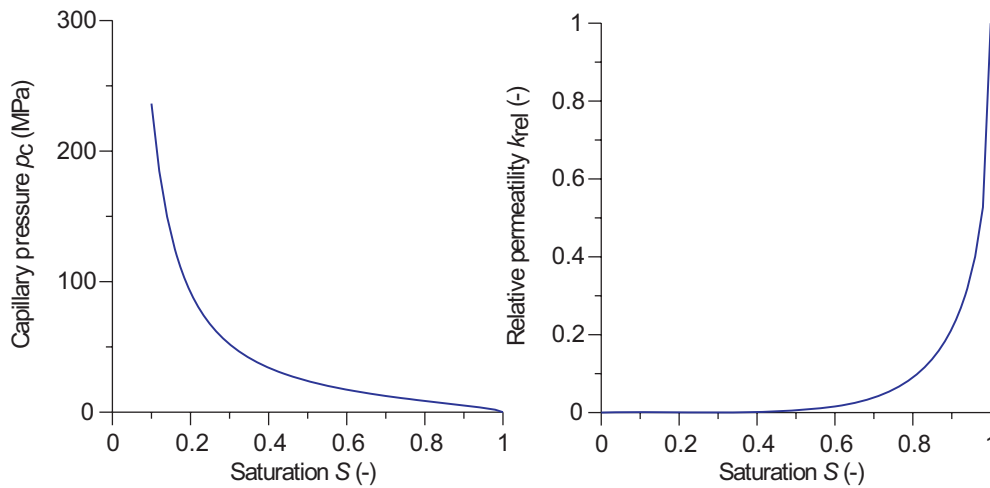


Figure 4.3: Capillary pressure p_c and relative permeability k_{rel} versus saturation S

Table 4.3: Porosity - Permeability relationship for argillite

Porosity (-)	Permeability (m ²)
0.03	1.0 · 10 ⁻¹⁹
0.05	1.0 · 10 ⁻¹⁸
0.075	2.125 · 10 ⁻¹⁸
0.125	4.375 · 10 ⁻¹⁸

4.4 Definition of simulated cases

The given problem has a complex initial stress state, time-dependent boundary conditions and material behaviour. To get an idea of the influence of the different processes we solve the problem stepwise. We start to analyze the processes induced by time-dependent saturation for the linear elastic case without considering any change in material properties. After that, we incorporate changes of porosity and permeability caused by time-dependent saturation and swelling/shrinking of the material. In a further step, we investigate the effect of initial stresses.

Table 4.4 gives a short overview of the cases that will be described in the following sections.

Table 4.4: Definition of three cases

Case number	Capillary pressure	Swelling/shrinking	Permeability $k_i = f(n)$	Initial Stresses	Simulation time
Case 1 : Influence of capillary pressure (CP)					
1	X	-	-	-	2 years
Case 2: Influence of swelling (CP/SW)					
2	X	X	X	-	2 years
Case 3: Consideration of initial stresses (CP/SW/IS)					
3	X	X	X	X	2 years

We simulate the following cases with time-dependent saturation. The simulation time is two years plus an assumed excavation phase of 15 days (total 745 days) with time steps of one day and the time-dependent saturation is shown in Figure 4.4. It starts with the initial state of saturation of 100.0 % at a pore pressure of 0.5 MPa. During the excavation phase the saturation decreases linearly to the mean value of 77.5 %, followed by a sinusoidal evolution, with a maximum value of 95 % and a minimum of 60 %. Mathematically it can be expressed as

$$S(t) = 0.175 \cdot \sin\left(\frac{2\pi}{365} t\right) + 0.775 \quad (4.13)$$

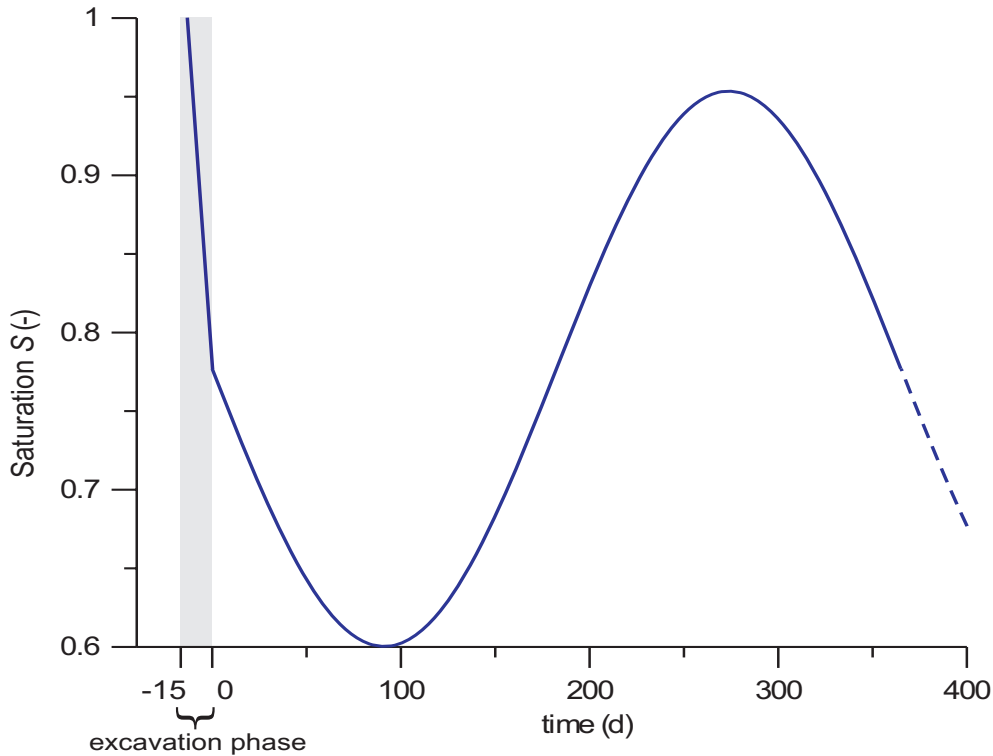


Figure 4.4: Time-dependent saturation S at the boundary of the tunnel

4.5 Results of simulated cases

Result of the simulation of Case 1 (CP) shows, that a change of saturation at the boundary of the tunnel influences a region around the tunnel with time. In the near field of the tunnel, the effect of seasonal fluctuation is high; whereas at distance the mean value is valid. This result is controlled by the boundary conditions, the permeability and the relation between the capillary pressure and the saturation.

The boundary conditions and material properties for Case 2 (CP/SW) are same as those of Case 1. Additionally, we assume a linear swelling model (see Table 4.1) and linear relationship between porosity and permeability (see Table 4.3).

4.5.1 Influence of swelling

In order to show the influence of swelling on the stresses of the rock mass surrounding the tunnel, Case 1 (CP, without swelling) and Case 2 (CP/SW, with swelling and change of porosity) are compared. The results are given for the closed up area (40m x 16.4m) in the large model area (80m x 40m). The stress fields are presented in Figure 4.5 and show that the incorporation of swelling leads to a different stress field. While the results for Case 1 (CP) are in the range of compressive stresses, in Case 2 (CP/SW) high values of tensile stresses are reached in the near field of the tunnel. These simulations are based on the assumptions of the swelling model and give only qualitative results. In spite of that, the results show that the swelling process may lead to tensile stresses in the rock surrounding the tunnel.

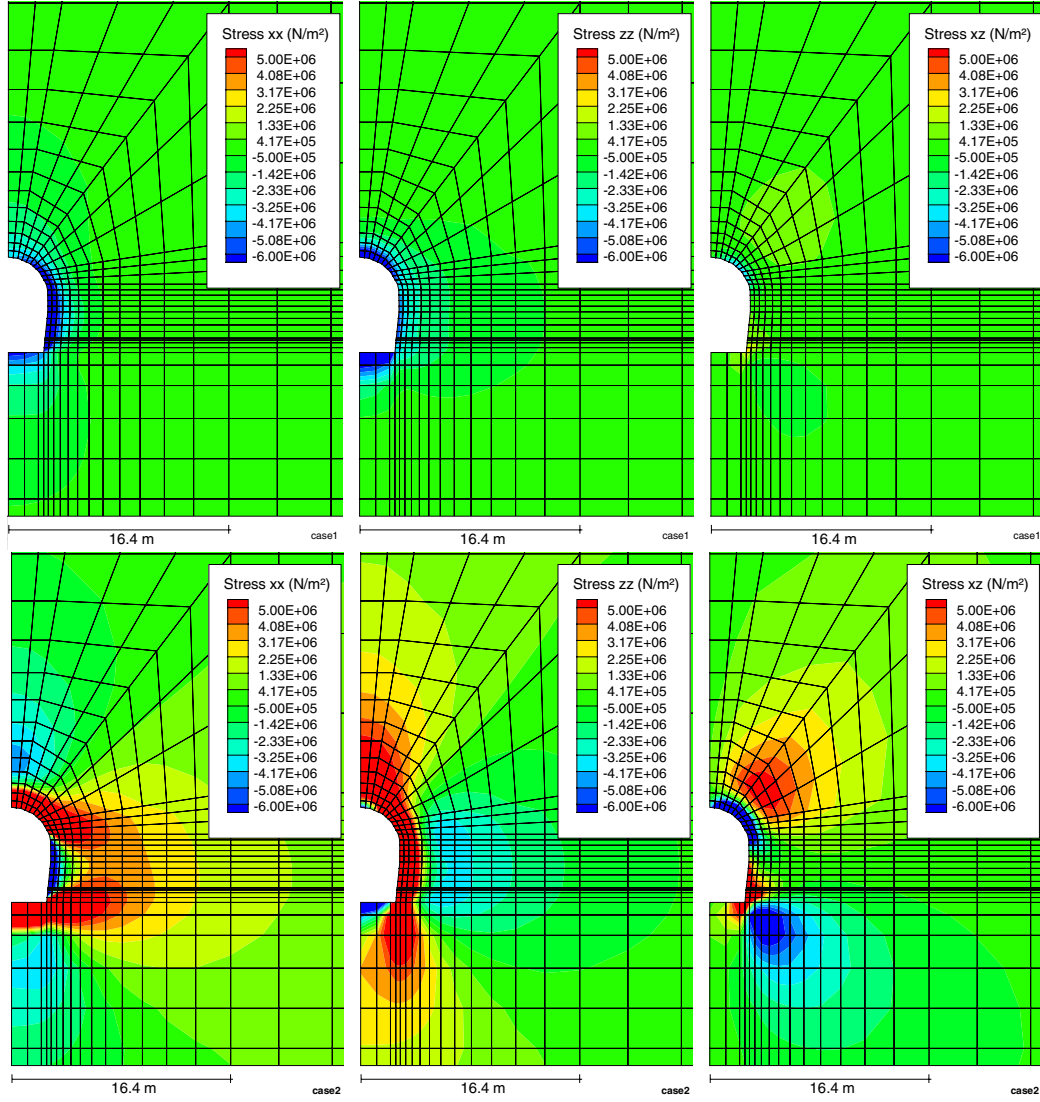


Figure 4.5: Stresses (Pa) after 1/4 years for case 1 (top) and case 2 (bottom)

4.5.2 Influence of initial stress field

In order for the initial stress field to be superimposed on to the stress field resulting from calculations of Case 2 (CP/SW), the initial conditions have to be specified. In a first step we assume an isotropic compressive stress field with stress magnitude

$$\sigma_{xx} = \sigma_{zz} = -4.32 \text{ MPa.} \quad (4.14)$$

The resulting stress fields for the two cases are presented in Figure 4.6. For a better overview, the results for Case 2 (CP/SW) are given again. Comparing the results of Case 2 (CP/SW) and Case 3 (CP/SW/IS), the magnitude and locations of tensile stresses around the tunnel are similar. The superposition of initial stresses attenuates the tensile stresses, so the range is more concentrate. The appearance of fractures in the near field of the tunnel, caused by tensile stresses, is likely. To get quantitative results, more information about the swelling process have to be incorporated in the model.

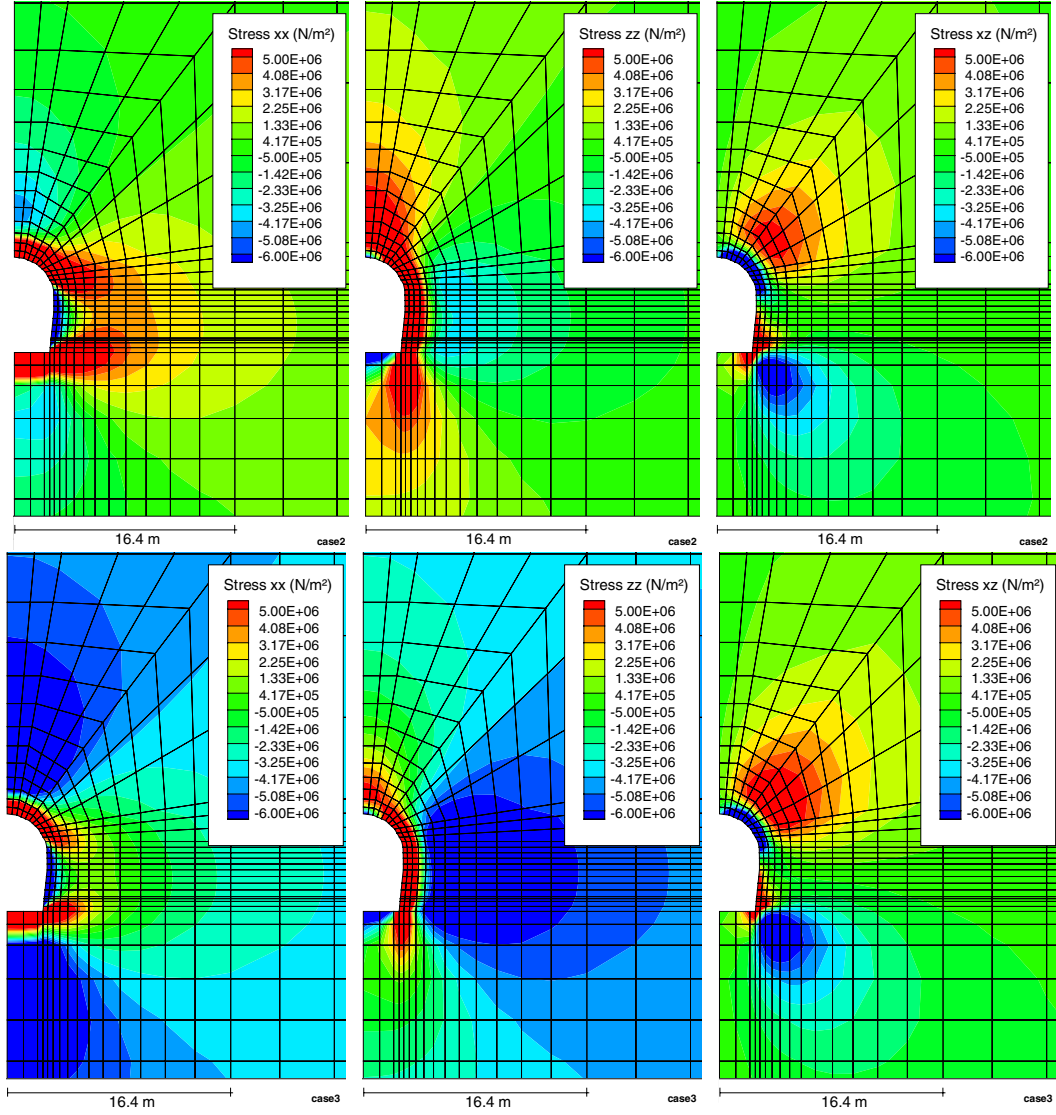


Figure 4.6: Stresses (Pa) after 1/4 years for case 2 (top) and case 3 (bottom)

4.5.3 Estimation of failure

A preliminary estimation of possible failure for the prediction of the EDZ is performed by evaluating the response from applying the yield criterion in an elastic analysis, disregarding any plastic or viscoelastic response. Thus, the predicted zone of possible failure is only an indication; its extent might be under- or overestimated in this first elastic analysis.

Here, we consider the parameters of Case 3 (CP/SW/IS). Additionally, the Mohr-Coulomb failure criterion is used. The yield function F bounding the elastic domain ($F < 0$) is

$$F(\sigma_1, \sigma_3) = (\sigma_1 - \sigma_3) + (\sigma_1 + \sigma_3) \sin \phi - 2 C \cos \phi = F(I_1, J_2, J_3) \quad (4.15)$$

where σ_1 and σ_3 are the principle stresses, C is the cohesion (1.4 MPa) and ϕ is the angle of internal friction (20°).

The resulting zone of indicated failure ($F > 0$) is depicted in Figures 4.7 and 4.8 directly after excavation and after 1/4 year, respectively. It is apparent that the initial failure zone is enlarged during the desaturation phase as the induced shrinking is accompanied by tensile stresses.

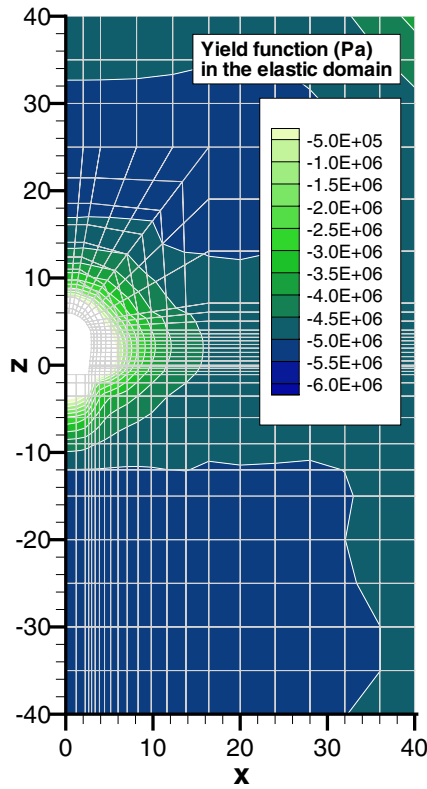


Figure 4.7: Initial time: function F in the elastic domain (colored) and extent of the failure zone (white)

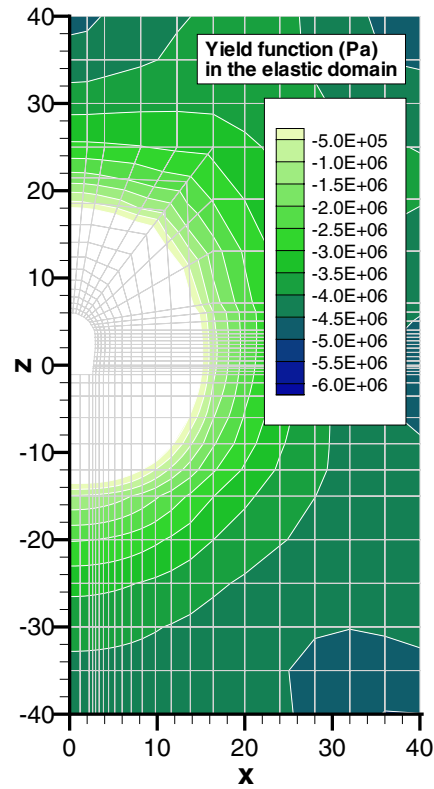


Figure 4.8: After 1/4 year: function F in the elastic domain (colored) and extent of the failure zone (white)

4.6 Synthesis

In Task 1C the ISEB/BGR team studied three cases with the consideration of three aspects: capillary effects, swelling/shrinking and incorporation of initial stresses. The results of Case 1 (temporal saturation and desaturation of near field rock) show the influence of the periods of saturation and desaturation on the pore water. Depending on the season, the tunnel wall region becomes saturated or desaturated. This causes a positive pressure gradient in radial direction for the saturation case and a negative pressure gradient for the desaturation case. At a farther distance, the rock remains in a desaturating phase, caused by the gradient between the outer and the inner boundary conditions, respectively $S = 1.0$ and $S = 0.775$. For the given material properties, the distinct influence of desaturation after 2 years takes place in a radius about 20 m from the tunnel wall.

Case 2 (influence of swelling) incorporates the swelling or shrinking of the clay. This effect has significant influence on the stresses and displacements in the area around the tunnel. Saturation causes swelling of the material and an increase of stresses. Without consideration of swelling, the rising saturation results in a decrease of stresses as the

capillary pressure decreases. Consequently, the results for cases with or without swelling are contrary to each other. The shrinking of the material leads to tensile stresses in the near field of the tunnel. In order to incorporate the influence of swelling and shrinking on long term properties, a non-linear swelling model has to be implemented.

Case 3 (consideration of initial stress field) includes the magnitude of the initial stress field in the simulation. As could be expected, a compressive initial stress field attenuates the tensile stresses. Nevertheless, close to the tunnel, zones with high tensile stresses can be observed. The appearance of fractures in the near field of the tunnel, caused by tensile stresses, is plausible. Considering the wide range of measured material properties, we repeat the simulation (case 3) assuming a reduction of the permeability about three orders of magnitude. A comparison of the results shows a decrease of the influence area with about a factor 10. The process of desaturation in the far field of the tunnel is not completed after 2 years. To reach a steady state condition, long term analysis is needed.

Based on results obtained from Case 3, a failure analysis is carried out from applying the yield criterion of Mohr-Coulomb in the poroelastic analysis with regard of swelling effects. If we consider the residual value of the cohesion of the material, the results show a time-dependent and increasing region of possible failure around the tunnel.

5 EDZ modelling by KU/JAEA team

5.1 Introduction

The argillaceous rock in the Tournemire site has several characteristic properties, and some of them have to be responsible for the mechanism of the EDZ around the tunnel. Anisotropy is possibly one of them. Laboratory tests and in-situ measurements indicate that the argillaceous rock at the site is anisotropic with respect mechanical properties from the bedding planes, which are nearly parallel to horizontal plane. Swelling properties of clay minerals also could be the important factor. The rock at this site includes smectite, and might show swelling-shrinking behaviour, as saturation changes. As a first step, the KU/JAEA team performed mechanical modelling with elastic isotropic or anisotropic properties, by using the further-developed finite element code THAMES. Also they have performed hydraulic modelling at unsaturated conditions. The specifications of the simulations and the results of Task C1 are presented in the report submitted by Uehara et al., (2005). This section summarizes their results.

5.2 Code development

THAMES (Thermal, Hydraulic and Mechanical System analysis) is a three-dimensional finite element code designed to analyze fully coupled thermal, hydraulic and mechanical behaviours of saturated and unsaturated geological materials. This code has been originally developed by Ohnishi et al. (1985), and later extended to be applicable to swelling material such as bentonite (Chijimatsu et al., 2001).

In this code, the change of the total stress tensor $\Delta\sigma_{ij}$ is given by:

$$\Delta\sigma_{ij} = -\frac{1}{2}C_{ijkl}(\Delta u_{k,l} + \Delta u_{l,k}) + \chi\Delta p\delta_{ij} + \Delta\sigma_{sw}\delta_{ij} + \beta\Delta T\delta_{ij} \quad (5.1)$$

where C_{ijkl} is the elastic modulus tensor [Pa], u_i is displacement vector [m], p is pore pressure [Pa], σ_{sw} is swelling pressure [Pa], β is a parameter related to thermal pressure [Pa/K], and T is temperature [K]. χ is saturation in the case of non-swelling material, and in the case of swelling material, χ is 1 at saturated condition and 0 at unsaturated condition.

The Flux vector q_i [kg/m³/s] at saturated condition is given by:

$$q_i = -\rho_w k_{ij} h_{,j} \quad (5.2)$$

and at unsaturated conditions

$$q_i = -\rho_w r_k k_{ij} h_{,j} - \rho_w (D_T)_{ij} T_{,j} \quad (5.3)$$

where ρ_w is water density [kg/m³], k_{ij} is permeability tensor [m/s], h is total head [m], r_k is relative permeability, and $(D_T)_{ij}$ is moisture diffusivity by thermal gradient.

The equations are discretised in space by applying the standard Galerkin method and finite difference method is applied to the discretization in time.

For this first step of Task C, the following simplified assumptions are considered:

- Swelling pressure is not considered; the material is assumed to be non-swelling.
- Thermal effect is not considered.
- The material is purely elastic.

For modelling work, a 2-D model with a plane strain condition is developed. For mechanical calculations, vertical and horizontal stress of 4 MPa is applied and there are no shear stresses applied. For hydraulic calculations, the total head of 0.5 MPa is used.

5.3 Mechanical modelling

To express the relationship between the failure criteria and stress conditions, the team calculated the ratio of the radius of Mohr circle, R , to the distance between the failure criteria and the center of Mohr circle (Figure 5.1). When the ratio R/D is less than 1, failure is not predicted; while, when R/D is more than 1, failure is predicted.

Two elastic mechanical calculations with isotropic and anisotropic properties are operated.

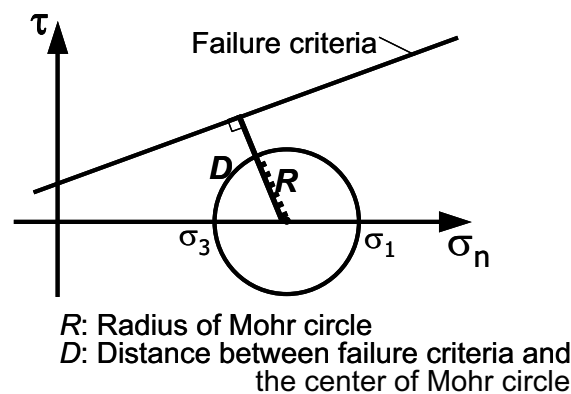


Figure 5.1: Mohr-Coulomb failure criteria and definition of R and D

5.3.1 Mechanical modelling with isotropic elastic properties

In this case where isotropic elastic properties are assumed, the following parameters are used: $E = 18\,000$ MPa, $\nu = 0.20$ and $\phi = 20^\circ$. For the cohesion used in the failure criteria, the three values of 10.8 MPa, 6.6 MPa and 1.4 MPa (residual cohesion) are used in the calculation.

Figure 5.2 shows the results of modelling when the cohesion failure criteria are 10.8 MPa and 6.6 MPa. We notice the high R/D domain distributed around the tunnel wall, especially at the top and the corner. However, no failure domain is predicted for these material conditions. In the case that the cohesion is 1.4 MPa failure is predicted around tunnel wall (Figure 5.3).

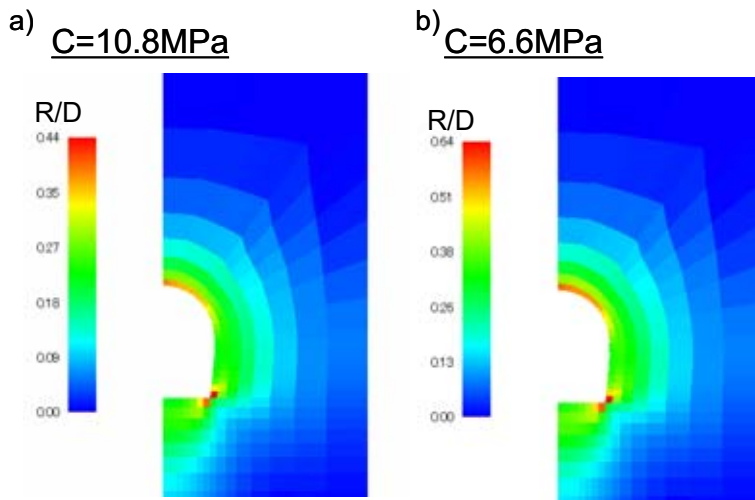


Figure 5.2: Predicted distribution of R/D ratio by using isotropic elastic properties

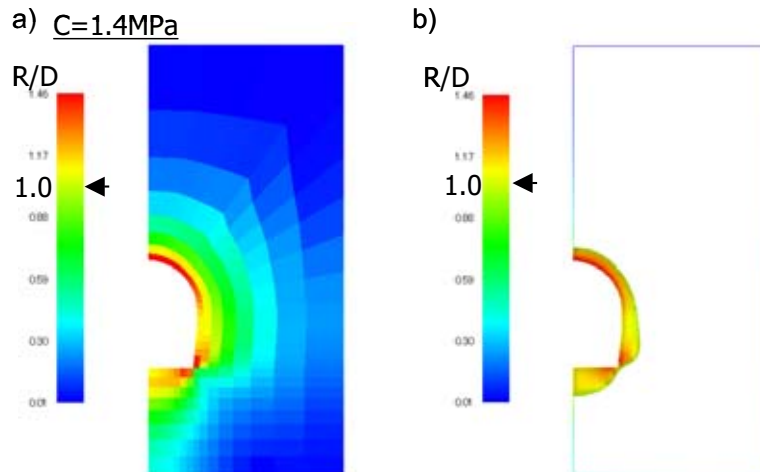


Figure 5.3: a) Predicted distribution of R/D ratio, b) Failure domain, in isotropic elastic case

5.3.2 Mechanical modelling with anisotropic elastic properties

In this case, the following elastic parameters, as defined in section 2.2.2, are used: $E_1 = 24.2$ GPa, $E_2 = 9.29$ GPa, $G_{12} = 3.94$ GPa, $\nu_{12} = 0.15$, $\nu_{23} = 0.2$

The cohesion of the Mohr Coulomb criteria depends on the angle from the bedding plane, θ , and is given in section 2.5.1

The maximum value of *cohesion*, C_{max} , is 10.8 MPa. The team also did modelling with C_{max} of 1.4 MPa.

When applying the failure criteria, the anisotropy of cohesion was taken into consideration in a simple way. The direction of maximum principal stress at each point in the calculation domain was calculated. Then, the cohesion from the given direction and the ratio R/D were calculated.

Figure 5.4 shows the result of modelling when C_{max} is 10.8 MPa. The distribution of the ratio R/D shows the difference from that of the isotropic case shown in Fig. 5.3, but

there are still no failure zone predicted. Figure 5.5 shows the results when $C_{max} = 1.4$ MPa. A failure domain is predicted in this case.

$C_{max}=10.8\text{MPa}$

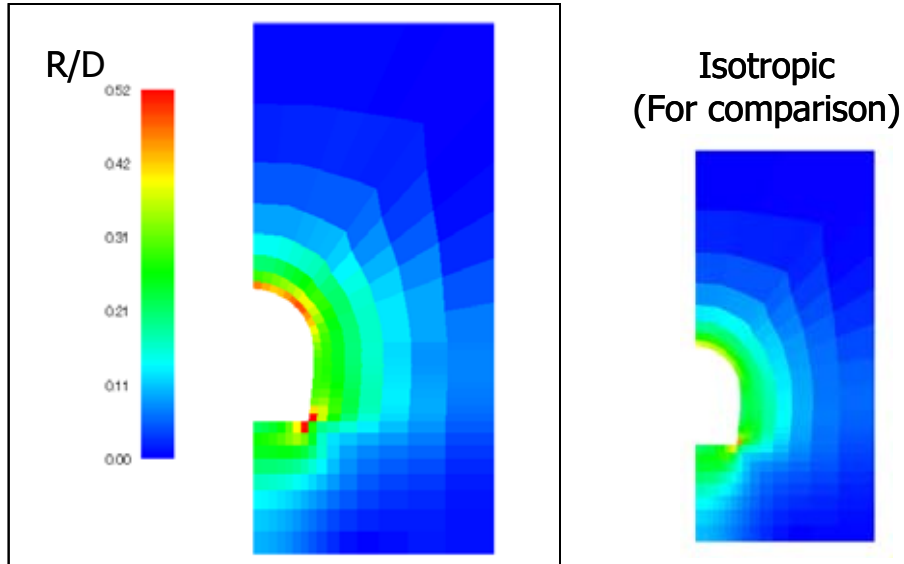


Figure 5.4: Predicted distribution of R/D ratio in the anisotropic calculation (left)

a) **$C_{max}=1.4\text{MPa}$**

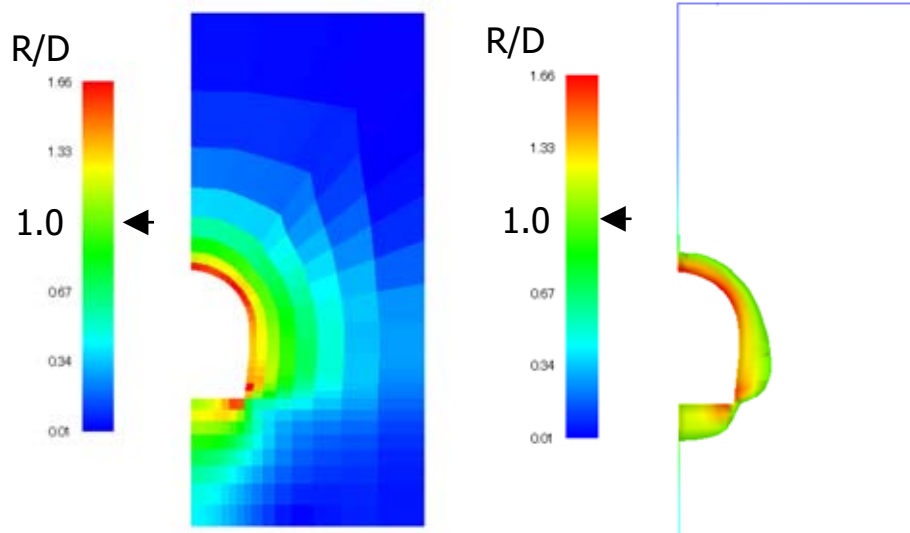


Figure 5.5: Predicted distribution of R/D ratio in the anisotropic calculation and for $C_{max}=1.4\text{MPa}$

5.4 Hydraulic modelling at unsaturated conditions

One of the possible factors related to the failure domain around tunnel wall is swelling-shrinking processes of clay minerals in the rock. This process is caused by saturation changes.

As a first step to investigate the possibility of importance of this factor at this site, the team simulated unsaturated hydraulic conditions and evaluated the development of EDZ domain where saturation change is predicted.

It is assumed that the whole calculation domain is initially saturated and the total head is 0.5 MPa, except for tunnel wall, which is assumed to be unsaturated. Observed humidity in the tunnel is oscillating between 40% and 95% (Rejeb et al., 2002). In the modelling the total head at tunnel wall is set to be -38 MPa, which corresponds to 76% relative humidity.

Intrinsic permeability and void ratio are defined as $1e-20$ m² and 0.085, respectively. The saturation-relative humidity relationship and saturation-suction relationship used are shown in Figure 5.6. The relationship depicted in figure 5.6a is based on laboratory data, whereas the relationship shown in Figure 5.6b is not from site data.

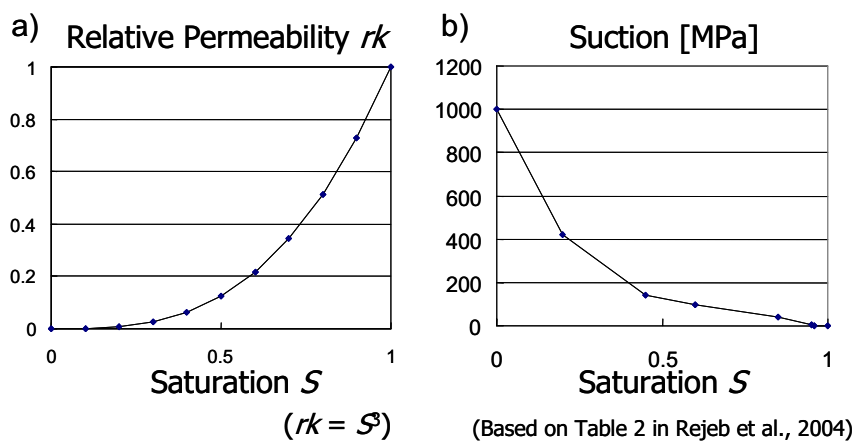


Figure 5.6: Relative permeability (a) and suction (b) versus saturation

Figure 5.7 shows distribution of predicted saturation ratio at each time step. The unsaturated domain is expanding from tunnel wall gradually as time evolves, and the expansion of the domain generally does not depend on the direction.

To observe the change of the distribution of saturation ratio, a plot of saturation along the profiles is shown in Figure 5.8. These results show that an unsaturated domain expands up to a few meters from tunnel wall in a year or less. For this condition, saturation change could be predicted in a domain within 1 meter or several tens cm from tunnel wall.

5.5 Synthesis

As a first step to approach Task C of DECOVALEX-THMC, the KU/JAEA team have performed pure elastic mechanical modelling with isotropic and anisotropic properties, together with hydraulic modelling assuming unsaturated condition for the argillite.

The results of mechanical modelling indicated that no failure zone is obtained for the modelling cases using isotropic and anisotropic elastic properties, when the Mohr Coulomb failure criteria derived from peak stresses are applied. Therefore, other mechanisms to explain the fracture zone (EDZ) observed at the tunnel wall must be developed and applied.

The results of hydraulic modelling suggest that the change of saturation ratio at the tunnel wall could affect saturation ratio of a domain to a depth of a few meters from the

tunnel wall after one year. This prediction supports the hypothesis that seasonal changes of humidity in the tunnel causes swelling-shrinking of the rock in a domain within several tens of cm from tunnel wall. Possibly this phenomenon is a likely mechanism for the production of fracture zone.

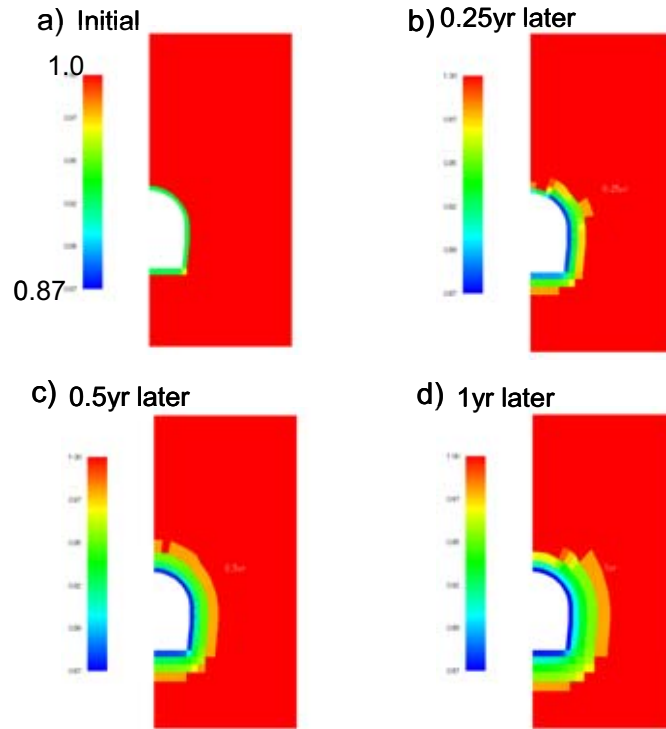


Figure 5.7: Predicted distribution of saturation ratio at four times

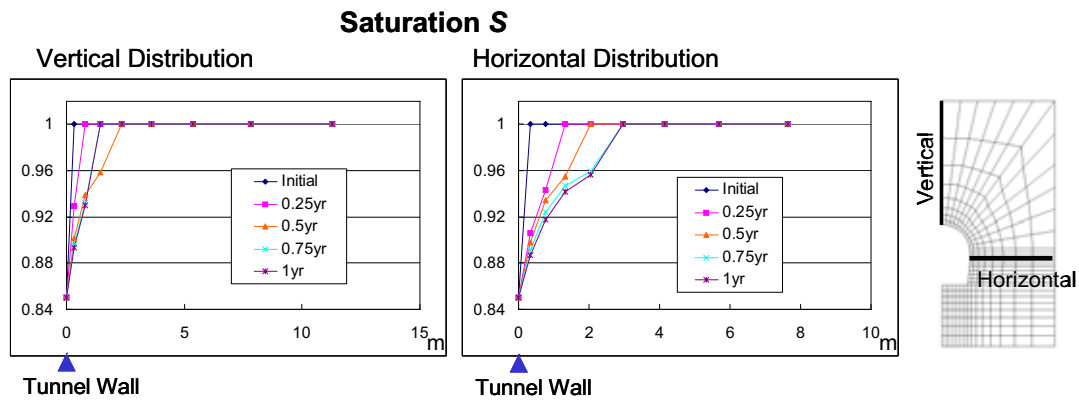


Figure 5.8: Predicted profiles of saturation along vertical and horizontal lines

6 Discussion and conclusion

In order to understand the main mechanisms governing the development of the EDZ around the old tunnel (Task C1), a considerable amount of modelling was carried out. The modelling performed by each research team depends on the capabilities of the codes and the human resources used.

The CEA/IRSN team carried out three different kinds of calculations: a pure mechanical calculation, a coupled hydro-mechanical calculation assuming saturated conditions, and a coupled hydro-mechanical calculation assuming unsaturated conditions. The ISEB/BGR team considered the hydro-mechanical approach at unsaturated condition by performing three simulation cases: influence of saturation/desaturation, influence of swelling/shrinking and influence of initial stress field on the development of the EDZ. The KU/JAEA team performed pure elastic mechanical modelling and hydraulic modelling at unsaturated condition.

The nature of this test case (understanding of the EDZ around the tunnel) does not make it possible to do a comparison of the results of the various teams, like what is normally done in the DECOVALEX project. Indeed, each team adopted their own approach to explain the EDZ in the rock next to the tunnel wall. Moreover, when the simulations from the different research teams are compared, it is seen that the parameters used in the calculations are different. We carried out a global analysis of the whole set of results in order to see whether they are coherence between them.

Concerning the elastic calculations, both CEA/IRSN and KU/JAEA team concluded that the EDZ only appears if the low residual cohesion of argillite is considered in the applied failure criterion. However, the shapes of the damaged zone predicted by these two teams are different. All the three teams calculated the extent of the unsaturated zone around the tunnel. The CEA/IRSN team estimates its extent to be 0.20 m for an intrinsic permeability of 10^{-19} m^2 . The ISEB/BGR team obtained an extent of approximately 20 m by considering a permeability of 10^{-18} m^2 . The K.U/JAEA calculated an extent of 2 m for permeability of 10^{-20} m^2 . It is known that the extent of unsaturated zone strongly depends on the value of the permeability. However, the results of the three teams are so inconsistent that further work is needed to check the differences. Perhaps the big differences are not surprising, given the very different assumptions used in this first effort by the teams. We expect their results will become more similar, as they reduce their assumptions to make their calculations more realistic.

Another difference in results is noted between the tensile stresses obtained from hydro-mechanical calculations by the two teams CEA/IRSN and ISEB/BGR. The calculation of the first team gives a tensile stresses about 20 MPa whereas the ISEB/BGR calculation show only 5 MPa near the wall of the tunnel.

Independently of these differences between the results, we can conclude that none of the linear or non-linear models used in Task C1 correctly predicts the form and the extent of the EDZ as observed around the tunnel at the Tournemire site. Moreover, observed fractures of the EDZ around the tunnel are mostly orthoradial, while the models tend to indicate different orientations corresponding to excessive shear stresses. Hence all the studies up to now point to the need of a new modelling strategy and incorporation of new physics to fully understand the EDZ development at the Tournemire site.

7 Perspective

Taking into account all the previous modelling work and the new results of the EDZ characterisation programme, a new modelling strategy is defined for the next sub-task, Task C2. The latest main investigations at the site concern the EDZ fracture patterns in the 1996 and 2003 drifts (cartography) and the fracture data from the radial boreholes (core analyses) in each opening. These investigations allow an accurate structural characterisation of the EDZs. The old tunnel has an EDZ with dense, homogeneous fracturing parallel to the tunnel wall, resembling onion skins. However, the new drifts do not have an EDZ similar to that of the tunnel. Unsaturated micro-cracks, mainly parallel to the bedding planes are observed on the non-covered walls of each drift. The extent of the EDZ does not seem to be affected by the age of the opening. It is approximately $0.2 R$, where R is the mean radius of the opening (drifts). In addition, the extent of the unsaturated zones slightly exceeds that of the fractured zones (EDZ) in the rock masses surrounding the three openings. For the old tunnel, masonry covering probably acted as a screen interrupting the advancement of the desaturation front around it.

Based on the new experimental characterisation work from the site, it can be assumed that the EDZ in the argillaceous rock at the Tournemire site is due to a deferred failure. At first, when the wall of the openings are not covered, the desaturation/resaturation phenomena induce tensile failure around the new drifts. Over time, the desaturation/resaturation phenomenon causes a gradual weakening of the material. The EDZ and fractures in the tunnel may then be explained by a hydraulic damage and a decreasing mechanical strength with the time followed by a mechanical failure of the damaged material. These assumptions remain to be confirmed or rejected through the current work of Task C. Indeed the next phase will be devoted to the prediction of the extent of the unsaturated zones around each of the openings at the site. Once these hydraulic calculations are validated by experimental data, we can estimate the EDZ around the new drifts by carrying out hydro-mechanical calculations for unsaturated conditions with subsequent change in mechanical properties. In particular, it can be of interest to use the time-dependent material laws with a very low strength over a failure zone of $0.2 R$, as observed at the site.

References

- Boisson J.Y., Cabrera J. & De Windt L. *Etude des écoulements dans un massif argileux, laboratoire souterrain de Tournemire*. Report EUR 18338FR, 1988.
- Cabrera J., Beaucaire C., Bruno G., De windt L., Genty A., Ramambasoa N., Rejeb A., Savoye S., Volant Ph. *Projet Tournemire. Synthèse des programmes de recherche 1995 - 1999*. Report IPSN/DPRE/SERGD 01 – 09. 2001.
- Chijimatsu, M., Fujita, T., Sugita, Y., Amemiya, K., and Kobayashi, A. *Field experiment, results and THM behaviour in the Kamaishi mine experiment*. Int. J. Rock Mech. Min. 38, pp.67-78, 2001.
- Daupley X., *Etude du potentiel de l'eau interstitielle d'une roche argileuse et de relations entre ses propriétés hydriques et mécaniques – application aux argilites du Toarcien dans la région de Tournemire*. PHD thesis of Paris School of Mines, December 5, 1997.
- Millard, A. and Rejeb, A. *DECOVALEX IV, Task C, Excavation Disturbed Zone (EDZ)*

- in the argillaceous Tournemire site (France)*. Progress report of CEA/IRSN team, March, 2005.
- Ohnishi, Y., Shibata, H., and Kobayashi, A. *Development of finite element code for the analysis of coupled Thermo-Hydro-Mechanical behaviours of a saturated-unsaturated medium*. Proc. of Int. Symp. on Coupled Process Affecting the Performance of a Nuclear Waste Repository, Berkeley, pp.263-268, 1985.
- Ramambasoa, N. *Etude du comportement hydromécanique des argilites – Application au site de Tournemire*. PHD thesis of Ecole Polytechnique, January, 10, 2001.
- Rejeb A. *Mechanical characterisation of the argillaceous Tournemire site (France)*. Proceedings of the international conference on rock engineering techniques for site characterisation. Oxford and IBH Publishing co. pvt. Ltd, p. 45 – 50. 1999.
- Rejeb, A., Pincent, B. and Robino, Ph. *Experimental evaluation of the termo-hydro-mechanical behaviour of the fractures in Tournemire site (France)*. Poster dans Clay in Natural and Engineered Barriers for Radioactive Waste Confinement, ANDRA, Reims, December 9, 12, 2002.
- Rejeb, A. *Time dependant behaviour of Tournemire argilites (France)*. Congrès International de Mécanique des Roches ISRM 2003, 8-12 Septembre, 2003, Gauteng, Afrique du Sud, p. 955-960. 2003.
- Rejeb, A. and Cabrera, Nunez, J. *DECOVALEX-THMC, DESCRIPTION FOR TASK C, Excavation Disturbed Zone (EDZ) in the argillaceous Tournemire site (France)*. Report DEI/SARG N°04-30. 2004.
- Uehara, S., Kobayashi, A., Chijimatsu, M. and Fujita, T. *DECOVALEX-THMC Task C*. Progress report of JAEA team, October, 2005.
- Vales, F., Nguyen, Minh D., Gharbi, H. and Rejeb, A. *Experimental study of the influence of the degree of saturation on physical and mechanical properties in Tournemire shale (France)*. Applied Clay Science 26 (2004), p. 197-207.
- Verpeaux, P., Millard, A., Charras, T. and Combescure, A. *A modern approach of large computer codes for structural analysis*. Proc SmiRT Conf, Los Angeles, USA. 1989.
- Ziefle, G., Kohlmeier, M., Maßmann, J. and Zielke, W. *DECOVALEX IV (THMC), Task C, Excavation Disturbed Zone (EDZ) in the argillaceous Tournemire site (France)*. Progress report of ISEB/BGR team, September, 2005.

www.ski.se

STATENS KÄRNKRAFTINSPEKTION
Swedish Nuclear Power Inspectorate

POST/POSTAL ADDRESS SE-106 58 Stockholm

BESÖK/OFFICE Klarabergsviadukten 90

TELEFON/TELEPHONE +46 (0)8 698 84 00

TELEFAX +46 (0)8 661 90 86

E-POST/E-MAIL ski@ski.se

WEBBPLATS/WEB SITE www.ski.se